J. Mech. Phys. Solids 206 (2026) 106342

Contents lists available at ScienceDirect

Journal of the Mechanics and Physics of Solids

journal homepage: www.elsevier.com/locate/jmps

Buckling and imperfection sensitivity of fluctuating one and two dimensional nanostructures

Xin Yan [a,*], Md Sojib Kaisar [b], Rubayet Hassan [b], Fatemeh Ahmadpoor [b,*]

[a] Advanced Manufacturing Center, Ningbo Institute of Technology, Beihang University, Ningbo 315100, PR China
[b] Department of Mechanical and Industrial Engineering, New Jersey Institute of Technology, Newark, NJ, United States

ARTICLE INFO

Keywords:
Entropy-driven mechanics
Thermal fluctuations
Buckling
Imperfection sensitivity
Two-dimensional materials

ABSTRACT

Thermal fluctuations significantly influence the mechanical behavior of low-dimensional elastic nanostructures due to their small bending stiffness. In this work, we develop a theoretical framework to investigate the buckling behavior of one- and two-dimensional flexible structures, namely, elastic rods and crystalline membranes, particularly when they experience large thermal fluctuations. Beginning with a thermally fluctuating elastic rod, we show that classical Euler buckling is recovered when geometric nonlinearities are neglected. Incorporating nonlinearities reveals substantial deviations in force–extension behavior, especially for rods with low bending stiffness. Extending the analysis to crystalline membranes, modeled through a nonlinear von Kármán elasticity of plate, we derive scaling laws for the critical buckling strain as functions of temperature, system size, and further explore their imperfection sensitivity. Our findings show that although imperfections can substantially alter the buckling threshold at zero Kelvin, their influence could be diminished at finite temperatures due to the presence of thermal fluctuations. Further, our results highlight the essential interplay between entropy-driven fluctuations and mechanical instabilities in low-dimensional systems, offering insights relevant to the design of thermally robust nanoscale materials and devices.

1. Introduction

Thin and slender structures, such as rods and membranes, are mechanically unstable under compressive loading, leading to buckling instabilities that are fundamental in both natural systems and engineered applications. At macroscopic scales, the onset of buckling can be well-described by classical theories of elasticity and stability, such as Euler's beam theory (Timoshenko, 1983) or the von Kármán plate model (Kármán, 1907). However, as the structural dimensions decrease to the micro- and nanoscale, new physical effects emerge that significantly alter mechanical response. In this regime, thermal fluctuations, geometric nonlinearities, and atomic-scale imperfections play a dominant role in determining the effective stability of elastic structures.

The mechanical behavior of low-dimensional materials is particularly sensitive to thermal fluctuations due to their reduced dimensionality and bending stiffness. For a filament (or membrane) at finite temperature, the ratio of thermal energy $k_B T$ to the characteristic bending energy κ/L (or κ_b) becomes non-negligible when the bending rigidity κ is small or the system size L is large. This places the structure in a fluctuation-dominated regime, where thermally induced undulations contribute significantly to configurational entropy and renormalize elastic moduli. Such effects are absent in classical zero-temperature continuum theories, but are essential for accurately modeling the mechanics of low-dimensional systems.

* Corresponding authors.
E-mail addresses: yan_xin@buaa.edu.cn (X. Yan), fatemeh.ahmadpoor@njit.edu (F. Ahmadpoor).

https://doi.org/10.1016/j.jmps.2025.106342
Received 25 May 2025; Received in revised form 27 July 2025; Accepted 2 September 2025
Available online 10 September 2025

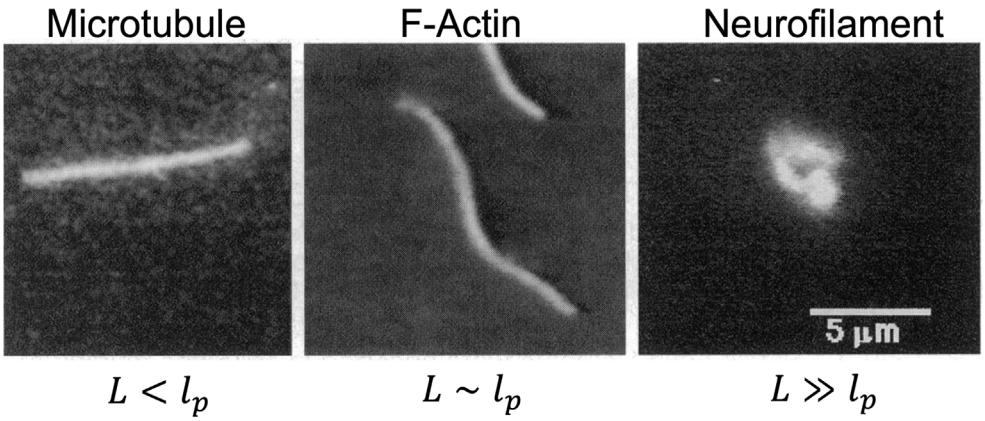

Fig. 1. Biological filaments span a broad mechanical spectrum, from stiff to flexible, enabling a wide range of structural and functional roles in cells. Stiff filaments, such as microtubules, exhibit persistence lengths on the order of millimeters, far exceeding their contour lengths, and thus behave as nearly rigid rods under physiological conditions. This mechanical rigidity enables them to serve as intracellular scaffolds and tracks for motor proteins (Gittes et al., 1993). Semiflexible filaments, such as actin filaments and intermediate filaments, have persistence lengths in the micrometer range (Gittes et al., 1993; Block et al., 2017), placing them in a regime where both thermal fluctuations and bending elasticity contribute significantly to their mechanical response. These filaments form dynamic cytoskeletal networks that can resist mechanical deformation while allowing for remodeling essential to processes like cell migration and division. In contrast, flexible filaments, such as neurofilaments, single-stranded RNA or intrinsically disordered protein regions, have persistence lengths of only a few nanometers (Hagerman, 1988), rendering them highly compliant and dominated by entropic elasticity. This flexibility facilitates functions that depend on conformational plasticity, including molecular recognition, gene regulation, and signal transduction. The mechanical diversity of biological filaments reflects the necessity for both structural stability and adaptability across cellular functions. Experimental pictures are from Käs et al. (1996).

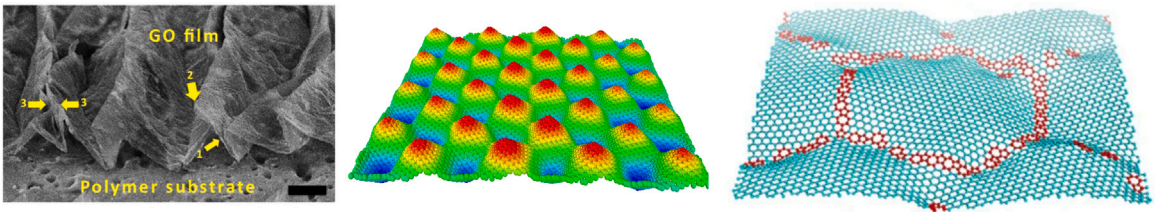

Fig. 2. Slender nanostructures can develop out-of-plane deformation patterns driven purely by mechanical instabilities. In particular, interactions with underlying substrates can induce wrinkle formation in crystalline membranes, as a result of mismatch stresses or mechanical confinement (Dai et al., 2020b; Ares et al., 2021; Dai et al., 2020a). Such wrinkling phenomena are not only of mechanical interest but also have functional implications in biomedical applications. (Right) Graphene-based surfaces with engineered wrinkle patterns have been demonstrated to serve as effective textured substrates for cell attachment, where the topographical cues introduced by wrinkling significantly influence cell alignment, morphology, and behavior (Wang et al., 2016).Out-of-plane deformation patterns maybe randomly or intentionally introduced on crystalline membranes for enhanced functionality. Defects and imperfections are inevitable in large-scale applications and are sometimes deliberately introduced to tailor the mechanical or physical properties of materials. For example, in graphene, it has been proposed that structural defects such as dislocations (Middle) and grain boundaries (Left) can induce local curvature in otherwise flat sheets, thereby enhancing toughness by redistributing stress and inhibiting crack propagation (Zhang et al., 2014; Shekhawat and Ritchie, 2016).

Semiflexible biopolymers, including actin filaments, microtubules, and intermediate filaments, exemplify this regime — see Fig. 1. These structures are characterized by a finite persistence length $\ell_p = \kappa/(k_B T)$, which quantifies the scale over which directional correlations decay. When the filament contour length L is smaller than ℓ_p, the filament behaves nearly rigidly; however, for $L \geq \ell_p$, thermal fluctuations induce significant configurational changes (Gittes et al., 1993; Block et al., 2017; Singh and Purohit, 2020; Argudo and Purohit, 2014; Su and Purohit, 2010). Such fluctuations are central to the mechanical function of the cytoskeleton, mediating cell shape, motility, and intracellular force transmission (Gov et al., 2003).

Similarly, nanoscale crystalline membranes such as graphene, MoS_2, MXenes, and biological lipid bilayers also exhibit strong thermal excitations due to their low bending stiffness (Gao and Huang, 2014; Chen and Kulkarni, 2017; Grasinger and Sharma, 2024; Ahmadpoor and Sharma, 2016a; Akinwande et al., 2017; Chen and Kulkarni, 2015; Hassan et al., 2024; Kaisar et al., 2025). These fluctuations strongly impact their mechanical behavior and response to external stimuli. For instance, nanoindentation experiments on suspended monolayer graphene reveal dramatic increases in apparent bending rigidity at micron scales—up to four orders of magnitude larger than the microscopic value (Blees et al., 2015)—as well as reductions in in-plane stiffness (Nicholl et al., 2017). These observations are consistent with predictions from statistical field theories and renormalization group approaches, which attribute the scale dependence of effective elastic moduli to entropy-driven out-of-plane undulations (Nelson and Peliti, 1987;

Ahmadpoor et al., 2017; Gao and Huang, 2014; Morshedifard et al., 2021). Notable efforts include the works by Morshedifard et al. (2021), Košmrlj and Nelson (2016), Bowick et al. (2017) and Hanakata et al. (2021) who showed that thermal fluctuations significantly enhance the effective bending rigidity of micron-scale fluctuating sheets, thereby increasing their critical buckling load. To investigate this quantitatively, they carried out coarse-grained molecular dynamics simulations on square sheets with varying sizes, elastic properties, and temperatures. Their results revealed that the presence of thermal fluctuations leads to a renormalized bending rigidity, causing the critical buckling load to scale with sheet size as $\sigma_{cr} \propto L^{-2+\eta}$, where $\eta \approx 0.8$ is a universal exponent reflecting this fluctuation-induced stiffening (Morshedifard et al., 2021). In biological systems, thermal fluctuations similarly govern the morphology and dynamics of lipid membranes, vesicles, and soft cellular compartments, influencing processes such as endocytosis, pore formation, and protein-membrane interactions (Lipowsky and Leibler, 1986; Lee et al., 2010; Farokhirad et al., 2021; Ahmadpoor and Sharma, 2016b; Hassan et al., 2025; Zelisko et al., 2017; Kulkarni, 2023; Ramesh and Kulkarni, 2024; Ahmadpoor et al., 2022, 2015).

While much progress has been made in understanding thermally fluctuating rods and membranes, the influence of both entropic factors and geometric imperfections on their mechanics remain less understood. Classical studies have shown that shell-like structures are highly sensitive to small geometric deviations, which can dramatically lower the buckling threshold (Hutchinson, 2016; Lee et al., 2016; Baizhikova et al., 2024). In nanoscale systems, imperfections are often unavoidable due to fabrication limits, topological defects, grain boundaries, or interactions with substrates (Zhang et al., 2014; Dai et al., 2020b; Shekhawat and Ritchie, 2016)—see Fig. 2. Moreover, these imperfections may not act independently of thermal fluctuations; rather, they may couple to entropic deformation modes, potentially suppressing or enhancing the effective imperfection sensitivity. Despite its practical importance, the interplay between thermal fluctuations and imperfections in nonlinear membranes remains poorly understood.

This work addresses this gap by developing a theoretical framework to investigate the buckling behavior of thermally fluctuating rods and membranes under compressive loading. Our approach integrates statistical mechanics with geometric nonlinear elasticity to capture the effects of entropy, nonlinear elasticity, and imperfections on mechanical stability. We investigate elastic rods and crystalline membranes as representative examples of one- and two-dimensional structures, respectively, and analyze how their buckling thresholds are influenced by temperature, system size, and the amplitude of defect-induced imperfections.

The main contributions of this paper are as follows:

- In Section 2, we revisit the classical buckling of a slender elastic rod within a statistical mechanical framework. We first consider the idealized case of a thermally fluctuating but geometrically linear rod. Using fluctuation spectrum analysis, we derive the critical compressive force and recover the Euler buckling result in the zero-temperature limit.
- Recognizing that soft filaments undergo large deformations, we incorporate geometric nonlinearities into the model and analyze the force–extension behavior of a semiflexible filament. Our analysis shows that at finite temperature and low bending stiffness, nonlinear effects play a critical role and substantially modify the buckling response.
- Section 3 extends the theoretical framework to two-dimensional structures, specifically crystalline membranes, modeled using a von Kármán-type formulation that captures the nonlinear coupling between in-plane strains and out-of-plane displacements. In this context, we examine not only the influence of thermal fluctuations on the buckling behavior but also the system's sensitivity to geometric imperfections at finite temperature. Prescribed initial imperfections are incorporated into the model, and scaling laws for the critical buckling strain are derived as functions of temperature, system size, and imperfection amplitude.
- Section 4 summarizes the key findings, discusses implications for the stability of nanostructured materials, and suggests directions for future work on the entropy-driven mechanics of flexible, low-dimensional systems.

2. Buckling of fluctuating semiflexible filaments

Semiflexible filaments are of central importance in both biological and synthetic systems, where their response to mechanical loads is critical for structural function. In biological contexts, key components of the cytoskeleton — namely microtubules, intermediate filaments, and actin filaments — are classified as semiflexible polymers. Experimental studies on *in vitro* microtubules (Brangwynne et al., 2006; Kurachi et al., 1995) and actin networks (Chaudhuri et al., 2007), including *in vivo* observations (Costa et al., 2002), have demonstrated that buckling under compression plays a crucial role in determining the mechanical response and stability of cellular structures. In addition, there is growing interest in the mechanical behavior of nanoscale synthetic filaments, such as carbon nanotubes, particularly under compressive loading (Falvo et al., 1997; Yap et al., 2007; Svenšek and Podgornik, 2008), with potential applications in targeted drug delivery systems (Bianco et al., 2005).

The classical buckling instability of rods under axial compression, first studied by Euler (1744), remains a foundational problem in elasticity. For a macroscopic elastic rod of length L and bending rigidity κ, clamped or pinned at both ends, the critical compressive force at which buckling occurs is given by $F_c = \pi^2\kappa/L^2$ (Landau and Lifshitz, 1986; Feynman et al., 1964). This threshold depends solely on the bending modulus is typically derived under the assumption of inextensibility. For slender bodies such as filaments or nanotubes with small radius r, a dimensional estimate shows that the ratio of bending to compression energy scales as $(r/L)^2$, justifying the neglect of compressibility in most cases (Landau and Lifshitz, 1986). Since biological and synthetic semiflexible filaments often have nanometer-scale radii and micrometer-scale lengths, the deformation response is dominated by bending.

When filaments are reduced to microscopic dimensions, the characteristic bending energy κ/L becomes comparable to the thermal energy scale k_BT. In this regime, entropic effects due to thermal fluctuations must be accounted for alongside classical mechanical energy. The inclusion of thermal contributions fundamentally alters the buckling behavior, lowering the critical force and introducing new physics not captured by zero-temperature theories. The present study aims to address this by developing a

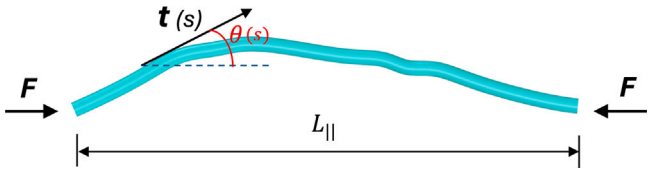

Fig. 3. Schematic of a semiflexible filament under compressive force **F**.

statistical mechanical framework for filament buckling at finite temperature, incorporating both the effects of bending stiffness and thermal fluctuations.

We consider an inextensible semiflexible filament of contour length L, subject to a homogeneous compressive force $\mathbf{F}$ (see Fig. 3). The filament is modeled within the wormlike chain framework (Boal and Boal, 2012), where the total energy comprises bending energy and the potential energy due to the external force. The Hamiltonian governing the filament configuration is given by

$$\mathcal{H} = \int_0^L ds \left[\frac{\kappa}{2} \left(\frac{d\mathbf{t}}{ds} \right)^2 - \mathbf{F} \cdot \mathbf{t}(s) \right], \tag{1}$$

where s is the arc-length parameter, $\mathbf{t}(s)$ is the unit tangent vector satisfying $|\mathbf{t}(s)| = 1$, and κ is the bending rigidity. The force $\mathbf{F}$ is assumed to act uniformly along the filament in a fixed direction. The inextensibility constraint can be satisfied identically by introducing a tangent angle field $\theta(s)$, such that $\mathbf{t}(s) = (\cos(\theta(s)), \sin(\theta(s)))$. Substituting this into the Hamiltonian yields

$$\mathcal{H} = \int_0^L ds \left[\frac{\kappa}{2} \left(\frac{d\theta}{ds} \right)^2 + F \cos(\theta(s)) \right], \tag{2}$$

where $F = |\mathbf{F}|$ is the magnitude of the compressive force. To quantify the filament's deformation under compression, we define the projected length in the direction of the applied force as

$$L_{\parallel} = \int_0^L \cos(\theta(s))\, ds, \tag{3}$$

which serves as a criteria for monitoring the buckling transition. In the straight configuration, where $\theta(s) = 0$, the projected length satisfies $L_{\parallel} = L$. Buckling leads to deviations from this value as the filament deforms transversely. The Hamiltonian formulated above provides the basis for analyzing the mechanical response of semiflexible filaments to compressive forces. The classical buckling point is determined by minimizing the energy in (2):

$$\kappa \frac{\partial^2 \theta}{\partial s^2} + F \sin(\theta) = 0. \tag{4}$$

By solving Eq. (4), the critical buckling force corresponding to the nth mode, denoted by F_c, is given by:

$$F_c = \frac{\pi^2 n^2}{L^2} \kappa. \tag{5}$$

Eq. (5) can be also obtained by studying the stability of the fluctuations spectra. To derive the fluctuations spectra for a semiflexible filament under compressive force, we start with expanding the orininal Hamiltonian in Eq. (2) up to the quadratic order as:

$$\mathcal{H}^q = \int_0^L ds \left[\frac{1}{2} \kappa \left(\frac{d\theta}{ds} \right)^2 - \frac{1}{2} F \theta^2 \right], \tag{6}$$

where the constant term FL is of no interest and thus not included. To discretize the Hamiltonian, we expand the angle θ into Fourier space as:

$$\theta(s) = \sum_{n=1}^{N} \bar{\theta}_n \exp(\imath n \pi s / L), \tag{7}$$

where $\bar{\theta}_n$ is the inverse Fourier transform. Substituting the Fourier transform into (6) gives us:

$$\mathcal{H}^q = \frac{L}{2} \sum_{n=1}^{N} \left[\kappa \left(\frac{n\pi}{L} \right)^2 - F \right] |\bar{\theta}_n|^2. \tag{8}$$

Then, using the equipartition theorem (Kittel, 2004) the correlation function can be obtained as:

$$\langle \bar{\theta}_n \bar{\theta}_m \rangle = \frac{k_B T L}{\kappa \pi^2 n^2 - F L^2} \delta_{n,m}, \tag{9}$$

where $\delta_{n,m}$ is the Kronecker delta signifying that the fluctuation modes are uncoupled. At the critical values of F_c, fluctuations in the nth mode become unstable. Setting the denominator in Eq. (9) to zero yields these critical forces, which match the values obtained

from Eq. (5). In other words, analyzing the stability of the fluctuation spectrum provides an alternative route to understanding the filament's buckling behavior. To track the force–deflection response, we also monitor the ensemble-averaged projected length $L_\parallel$:

$$\begin{aligned}\langle L_\parallel\rangle &= \int_0^L \langle\cos(\theta)\rangle ds = \int_0^L \langle 1-\frac{\theta^2}{2}+\frac{\theta^4}{24}+\cdots\rangle ds \\ &= L\left(1-\frac{\langle\theta^2\rangle}{2}+\frac{\langle\theta^4\rangle}{24}+\cdots\right)\end{aligned} \tag{10}$$

The deviation of the projected length from the contour length can be expressed in normalized form as:

$$\begin{aligned}1-\frac{\langle L_\parallel\rangle}{L} &= \frac{\langle\theta^2\rangle}{2}-\frac{\langle\theta^4\rangle}{24}+\cdots = \frac{\langle\theta^2\rangle}{2}-\frac{\langle\theta^2\rangle^2}{8}+\frac{\langle\theta^2\rangle^3}{48}+\cdots \\ &= \sum_{k=1}\frac{(-1)^{k+1}(2k-1)!!}{(2k)!}\langle\theta^2\rangle^k = \sum_{k=1}\frac{(-1)^{k+1}(2k-1)!!}{(2k)!}\left(\sum_{n=1}^{N}\frac{k_BTL}{\kappa\pi^2n^2-FL^2}\right)^k,\end{aligned} \tag{11}$$

where we have used the Wick's theorem[1] to calculate the higher order correlation functions (Kleinert, 1989). In the absence of any external force, i.e. $F=0$, and within quadratic approximation, the expression in (11), reduces to:

$$1-\frac{\langle L_\parallel\rangle}{L}\approx\frac{\langle\theta^2\rangle}{2}=\frac{1}{2}\sum_{n=1}^{N}\langle|\bar{\theta}_n|^2\rangle=\frac{k_BTL}{2\kappa\pi^2}\sum_{n=1}^{N}\frac{1}{n^2}=\frac{k_BT}{12\kappa}L=\frac{L}{12\ell_p}. \tag{12}$$

In Eq. (12), the summation is evaluated in the limiting case as $N\to\infty$, and the ratio $\ell_p=\kappa/(k_BT)$ defines the persistence length (Boal and Boal, 2012), which characterizes the influence of thermal fluctuations on the filament's configuration. For large ℓ_p (i.e., stiff filaments or low temperatures), the projected length closely approximates the contour length. In contrast, for small ℓ_p (i.e., flexible filaments or high temperatures), the deviation becomes significant. The normalized shrinkage in Eq. (12) depends on the ratio L/ℓ_p, indicating that thermal fluctuations become prominent when the filament length greatly exceeds its persistence length, and negligible when it is much smaller.

In calculating the critical buckling force at zero temperature (ground state), it is typically assumed that the elastic rod is perfectly straight and that, near the buckling point, the deflection angle θ is small enough to justify the approximation $\cos\theta\sim1-\theta^2/2$ (or $\sin\theta\approx\theta$). However, at finite temperature and particularly for semiflexible and flexible filaments, thermal fluctuations can cause large deviations, rendering this approximation invalid. In such cases, it becomes necessary to expand $\cos(\theta)$ in the original energy (2) to higher-order terms as below:

$$\mathcal{H}=\int_0^L ds\left[\frac{1}{2}\kappa\left(\frac{\partial\theta}{\partial s}\right)^2+F\left(1-\frac{1}{2}\theta^2+\frac{1}{24}\theta^4\right)\right]. \tag{13}$$

In the following, we use the above quartic energy function to examine the buckling instability of a *fluctuating* semiflexible filament. The presence of the quartic term prevents the application of the equipartition theorem for calculating the partition function and fluctuations and, consequently, the force–deflection response. To address this, we employ an approximate approach based on variational perturbation theory (VPT) (Kleinert, 1989, 2009; Ahmadpoor et al., 2017), which allows us to implement the effects of geometric nonlinearities (nonquadratic terms) in our statistical mechanics model. In this method (See Appendix), a trial quadratic energy functional is optimized to approximate the original non-quadratic energy, enabling the use of the equipartition theorem to compute thermal fluctuations.

To start, let the trial energy function in Fourier space be

$$U_0=L\sum_{n=1}^{N}G(n)|\bar{\theta}_n|^2 \tag{14}$$

where $G(n)$ is the unknown coefficient and needs to be optimized. The original energy can then be rewritten as:

$$U=U_0+\delta\left(\mathcal{H}-U_0\right) \tag{15}$$

where δ should be set to 1 at the end for which the right and left hand sides will be the same as the original nonlinear Hamiltonian $\mathcal{H}$. Following the VPT approach, we will treat the term $\delta\left(\mathcal{H}-U_0\right)$ as a small nonlinear perturbation around U_0 and expand the free energy in Taylor series in orders of δ as below:

$$\mathcal{F}=\mathcal{F}_0-k_BT\sum_{k=1}^{\infty}\frac{(-\delta)^k}{n!(k_BT)^k}\langle(\mathcal{H}-U_0)^k\rangle_{U_0}^c \tag{16}$$

[1] According to Wick's theorem the higher order correlation function of any physical variable x, within quadratic Hamiltonian can be written as:

$$\langle x^{2n}\rangle=(2n-1)!!\langle x^2\rangle^n$$

.

where $\mathcal{F}_0$ is the free energy associated with the trial function (14) and the ensemble averages are presented in cumulants[2] and calculated with respect to the trial function U_0. Setting $\delta = 1$, the variational free energy $\mathcal{F}_{\text{var}}$ up to first order is given by

$$\begin{aligned}\mathcal{F}_{\text{var}} &= \mathcal{F}_0 + \langle \mathcal{H} - U_0 \rangle_{U_0} \\ &= \frac{1}{2} k_B T \sum_n \log(G(n)) + \frac{1}{2} L \sum_n \left[\kappa \left(\frac{n\pi}{L} \right)^2 - F \right] \langle |\bar{\theta}_n|^2 \rangle_{U_0} + \frac{1}{24} F L \langle \theta^4 \rangle_{U_0} + C_{\text{F}}\end{aligned} \tag{17}$$

where C_F is a constant of no consequences. The ensemble averages in (17) are calculated as

$$\begin{aligned}\langle |\bar{\theta}_n|^2 \rangle_{U_0} &= \frac{k_B T}{2LG(n)}, \\ \langle \theta^4 \rangle_{U_0} &= 3\langle \theta^2 \rangle_{U_0}^2 = 3 \left(\sum_{n=1}^{N} \langle |\bar{\theta}_n|^2 \rangle_{U_0} \right)^2 = 3 \left(\sum_{n=1}^{N} \frac{k_B T}{2LG(n)} \right)^2 = 3\eta^2\end{aligned} \tag{18}$$

where we defined $\eta = \sum_{n=1}^{N} \langle |\bar{\theta}_n|^2 \rangle_{U_0}$ for ease of notation. Substituting the ensemble averages in (18) into (17), we have

$$\mathcal{F}_{\text{var}} = \frac{1}{2} k_B T \log \left(\frac{LG(n)}{k_B T} \right) + \frac{L}{2} \sum_n \left[\kappa \left(\frac{n\pi}{L} \right)^2 - F \right] \frac{k_B T}{2LG(n)} + \frac{1}{8} F L \eta^2 + C_{\text{F}}. \tag{19}$$

Minimizing the sensitivity of the variational free energy $\mathcal{F}_{\text{var}}$ with respect to the trial function gives us the optimized expression for $G(n)$ to be used in a quadratic function:

$$\frac{\partial \mathcal{F}_{\text{var}}}{\partial G(n)} = \frac{k_B T}{G(n)} - \left[\kappa \left(\frac{n\pi}{L} \right)^2 - F \right] \frac{k_b T}{4G(n)^2} - \frac{k_B T F}{8G(n)^2} \eta := 0. \tag{20}$$

The solution to the above variational problem is given by

$$G(n) = \frac{1}{2} \left(\kappa \left(\frac{n\pi}{L} \right)^2 - F \right) + \frac{1}{4} F \eta. \tag{21}$$

Then, η can be obtained from the following implicit equation:

$$\eta = \sum_{n=1}^{N} \langle |\bar{\theta}_n|^2 \rangle_{U_0} = \sum_{n=1}^{N} \frac{k_B T}{2LG(n)} = \sum_{n=1}^{N} \frac{k_B T}{L \left(\kappa \left(\frac{n\pi}{L} \right)^2 - F + \frac{1}{4} F \eta \right)}. \tag{22}$$

To simplify the expression for η we normalize the force F by the critical buckling force at ground state: $F_{c,0} = \pi^2 \kappa / L^2$. Let $F = \bar{F} F_c$. Then η will be

$$\eta = \frac{k_B T}{F_c L} \sum_{n=1}^{N} \frac{1}{n^2 - \bar{F} + \frac{1}{2} \bar{F} \eta} = \frac{L}{\ell_p \pi^2} \sum_{n=1}^{N} \frac{1}{n^2 - \bar{F} + \frac{1}{4} \bar{F} \eta} \tag{23}$$

wherein we substitute $\frac{k_B T}{F_c L} = \frac{L}{\ell_p \pi^2}$. Once η is evaluated for a filament with given properties, the normalized end-to-end distance in (11) can be calculated as a function of applied force.

$$1 - \frac{\langle L_{\parallel} \rangle}{L} = \frac{\langle \theta^2 \rangle}{2} - \frac{\langle \theta^4 \rangle}{24} + \cdots = \sum_{k=1} \frac{(-1)^{k+1} (2k-1)!!}{(2k)!} \eta^k. \tag{24}$$

Some quantitative results are given in Fig. 4, where we plotted normalized end-to-end distance versus different values of normalized force $\bar{F}$. Note that $\bar{F} = 1$ corresponds to critical buckling force at ground state. As can be seen from the plot, the soft filaments have a smooth transition between pre-buckling and post buckling, while rigid filaments have a sharper transition. The results in Fig. 4 can be interpreted as following:

- At low temperatures, when the fluctuations are negligible, the buckling behavior is close to ground state solution.
- For small ratios of L/l_p, the filament behaves like a rigid bar, where the fluctuations are small and hence the buckling behavior is similar to that of low-temperature result.
- Soft filaments, on the other hand have a quite smooth transition during buckling and post-buckling. For both high-temperature case and large L/l_p ratio, the fluctuations have remarkable impact on the buckling behavior.

[2] The cumulant averages, up to fourth order, are:

$$\langle \mathcal{X} \rangle_{U_0}^c = \langle \mathcal{X} \rangle_{U_0}, \quad \langle \mathcal{X}^2 \rangle_{U_0}^c = \langle \mathcal{X}^2 \rangle_{U_0} - \langle \mathcal{X} \rangle_{U_0}^2, \quad \langle \mathcal{X}^3 \rangle_{U_0}^c = \langle \mathcal{X}^3 \rangle_{U_0} - 3\langle \mathcal{X}^2 \rangle_{U_0} \langle \mathcal{X} \rangle_{U_0} + 2\langle \mathcal{X} \rangle_{U_0}^3,$$
$$\langle \mathcal{X}^4 \rangle_{U_0}^c = \langle \mathcal{X}^4 \rangle_{U_0} - 3\langle \mathcal{X}^3 \rangle_{U_0} \langle \mathcal{X} \rangle_{U_0} - 3\langle \mathcal{X}^2 \rangle_{U_0}^2 + 12\langle \mathcal{X}^2 \rangle_{U_0} \langle \mathcal{X} \rangle_{U_0}^2 - 6\langle \mathcal{X} \rangle_{U_0}^4$$

.

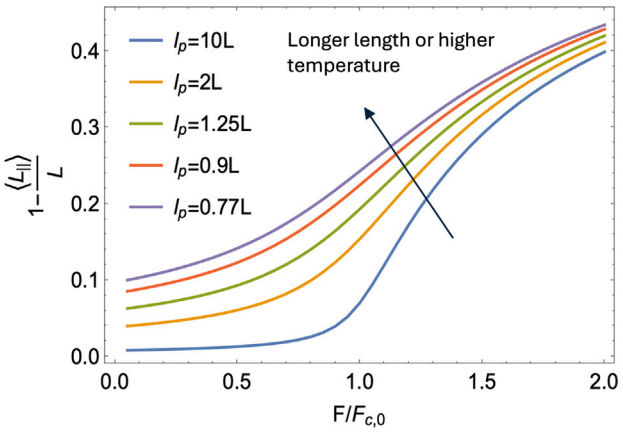

Fig. 4. Change of end-to-end distance versus normalized force. At low temperatures, where thermal fluctuations are minimal as well as for filaments with small ratios of contour length to persistence length ($L/l_p \ll 1$), thermal fluctuations are effectively suppressed. As a result, the filament behaves as a nearly rigid body, undergoing a sharp buckling transition analogous to that observed at zero temperature. In contrast, soft filaments with large L/l_p ratios enter a thermally dominated regime, where entropic effects play a central role in shaping the mechanical response. In this regime, the buckling transition is no longer abrupt but becomes smooth and continuous. These effects are particularly significant in biological filaments, where thermal fluctuations contribute to nonlinear behavior even in the pre-buckling regime, highlighting the importance of entropic contributions to mechanical stability.

The results presented in this section are qualitatively consistent with previous studies in the literature. However, a few earlier works have reported somewhat different observations. For example, Baczynski et al. (2007) described an intriguing phenomenon in which semiflexible filaments, in the post-buckling regime, exhibit a projected length greater than that of a rigid filament under the same normalized force. By integrating over all short-wavelength modes using a quadratic Hamiltonian, the authors derived an effective theory describing the buckling instability of the longest-wavelength Fourier mode. They further validated their findings through Monte Carlo simulations. In addition to differences in the analytical approach, the boundary conditions in their study differ from those employed here. Specifically, Baczynski et al. (2007) considered clamped and simply supported boundary conditions, which yield distinct eigenfunctions for the Fourier modes. In contrast, the present work adopts periodic boundary conditions, which inherently encompass eigenfunctions associated with both clamped and simply supported ends. We speculate that both the approximate analytical methods and the choice of boundary conditions contribute to the discrepancies in the results. This highlights the need for more rigorous studies on the buckling behavior of thermally fluctuating filaments.

Another notable contribution on this topic is the work by Su and Purohit (2012). In that study, the authors introduced a novel approach that integrates structural and statistical mechanics to investigate the entropic elasticity of semiflexible filament networks. They modeled the network as a frame structure and, in the first step, used structural mechanics to determine its static equilibrium configuration under applied loads. To incorporate thermal fluctuations around this equilibrium state, they approximated the potential energy of the deformed frame up to second order in the kinematic variables, yielding a deformation-dependent stiffness matrix that characterizes the network's flexibility. Using this stiffness matrix, they applied statistical mechanics to evaluate the partition function, free energy, and thermo-mechanical properties of the network. Notably, they demonstrated that penalty methods commonly used in finite element analysis to handle constraints remain applicable when combining statistical and structural mechanics in their framework. They applied this method to study the expansion, shear, uniaxial tension, and compression behavior of simple filament networks as well as imperfection-sensitivity of semiflexible filaments, successfully capturing stress-stiffening arising from filament reorientation and the suppression of thermal fluctuations, as well as reversible stress-softening associated with filament buckling. It is important to note that, although the results presented here are qualitatively consistent with the analysis of Su and Purohit (2012), their study is based on a fundamentally different assumption regarding the original Hamiltonian used to describe filament response. In contrast to the present work, Su and Purohit (2012) not only neglect the higher order terms in their Hamiltonian but also introduce an additional elastic modulus for the filament, analogous to the elastic modulus of a beam, which becomes relevant when the filament's contour length changes—either through compression or stretching—to the extent that thermal fluctuations are completely suppressed. This extra elastic contribution can significantly affect the overall mechanical response and behavior of a filament network at the extreme regimes of stretching or compression.

The physiological implications of these results depend on the filament's stiffness. Semiflexible filaments span a wide range of stiffnesses, characterized by their persistence lengths ℓ_p. Among cytoskeletal filaments, actin exhibits a persistence length of approximately 10–20 μm (Gittes et al., 1993), making it moderately stiff and responsive to both thermal and mechanical forces. Microtubules, in contrast, are significantly stiffer, with persistence lengths in the range of 1–5 mm (Gittes et al., 1993). DNA, a classic example of a semiflexible polymer, has a persistence length of about 50 nm under physiological conditions (Hagerman, 1988). Intermediate filaments such as vimentin are more compliant, with persistence lengths between 0.3 and 1 μm (Block et al., 2017). In the realm of synthetic materials, single-walled carbon nanotubes possess high bending stiffness with persistence lengths estimated

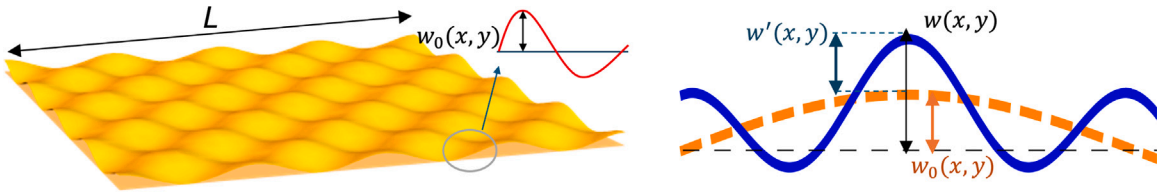

Fig. 5. Schematic of a fluctuating membrane with preexisting out-of-plane displacement field.

between 10 and 100 μm, depending on geometry and environment (Falvo et al., 1997). Engineered DNA origami filaments provide a programmable platform with tunable stiffness, exhibiting ℓ_p in the range of 1–3 μm (Dietz et al., 2009). These values highlight the broad mechanical spectrum of semiflexible filaments and their buckling behavior across biological and nanotechnological contexts.

3. Buckling and imperfection sensitivity of a fluctuating nonlinear elastic sheet

In this section, we examine how thermal fluctuations influence the buckling behavior and imperfection sensitivity of a nonlinear elastic sheet. Imperfections may arise from various sources, including material inhomogeneities, topological defects such as dislocations, or other irregularities like atomic vacancies and impurities. To begin, consider a planar, thin elastic sheet occupying a square domain $\mathbb{S} = (0, L)^2$ in the x–y plane. At zero temperature ($T = 0$ K), corresponding to the undeformed ground state, the sheet lies flat in the $z = 0$ plane. Each point on the sheet is identified by its position vector $\mathbf{x}$. Let $\mathbf{u}$ be a displacement field defined on $\mathbb{S}$, mapping each point from the undeformed configuration in the 2D plane to a corresponding point on the deformed surface in 3D space. The position vector of a point on the deformed surface is then given by $\mathbf{r} = \mathbf{x} + \mathbf{u}$. The deformation gradient associated with this mapping is defined as $\mathbf{F} = \nabla_{2D}\mathbf{r}$, which transforms 2D tangent vectors into their deformed 3D counterparts. Under this deformation, the sheet may undergo both in-plane stretching (or compression) and out-of-plane bending. These deformations are typically characterized using the first and second fundamental forms of the surface. The metric tensor $\mathbf{g}$, captures changes in the intrinsic geometry (i.e., the in-plane stretching) of the sheet and is given by $\mathbf{g} = \mathbf{F}^T\mathbf{F}$. The Green–Lagrange strain field is a 2D tensor and can be written as expressed as (Gurtin et al., 2010; Lu and Huang, 2009):

$$\mathcal{E} = \frac{1}{2}(\mathbf{g} - \mathbf{I}). \tag{25}$$

where $\mathbf{I}$ is the 2D identity tensor. In addition to the in-plane strain field, the sheet can experience bending deformation in the 3D space. Let $\mathbf{n}$ be the normal vector on the deformed surface. The curvature tensor is defined as

$$\mathbf{L} = -\nabla_{2D}\mathbf{n}.$$

The invariants of the curvature tensor are the mean H and Gaussian K curvatures and derived as (Biria et al., 2013):

$$H = \frac{1}{2}\mathrm{tr}(\mathbf{L}) = -\frac{1}{2}\mathrm{div}_{2D}\mathbf{n},$$
$$K = \frac{1}{2}\left((\mathrm{tr}(\mathbf{L}))^2 - \mathrm{tr}(\mathbf{L}^2)\right),$$

where tr denotes the trace of the tensor. We denote the components of the displacement field of the deformed sheet as: $\mathbf{u}(\mathbf{x}) = (u_x(\mathbf{x}), u_y(\mathbf{x}), w(\mathbf{x}))$. To incorporate the effects of imperfections, we introduce a preexisting out-of-plane displacement field, $w_0(\mathbf{x})$ as depicted in Fig. 5. Consequently, the total out-of-plane displacement can be expressed as the sum of this imperfection field and an additional fluctuation field:

$$w(\mathbf{x}) = w_0(\mathbf{x}) + w'(\mathbf{x}).$$

To induce and control buckling, we impose a compressive strain along a single direction — specifically, the y-axis. The nonlinear strain components are therefore:

$$\mathcal{E}_{xx} = \frac{\partial u_x}{\partial x} + \frac{1}{2}\left(\frac{\partial w}{\partial x}\right)^2, \quad \mathcal{E}_{yy} = \frac{\partial u_y}{\partial y} + \frac{1}{2}\left(\frac{\partial w}{\partial y}\right)^2 + \epsilon_0, \quad \mathcal{E}_{xy} = \frac{1}{2}\left(\frac{\partial u_x}{\partial y} + \frac{\partial u_y}{\partial x} + \frac{\partial w}{\partial x}\frac{\partial w}{\partial y}\right). \tag{26}$$

Assuming material isotropy, the corresponding elastic energy cost for the strain field can be written as a function of its principal invariants, $I_1(\mathcal{E}) = \mathcal{E}_{xx}^2 + \mathcal{E}_{yy}^2$ and $I_2(\mathcal{E}) = \mathcal{E}_{xx}\mathcal{E}_{yy}$ and $I_3(\mathcal{E}) = \mathcal{E}_{xy}^2$ as :

$$U_s = \int_{\mathbb{S}} \frac{E}{2(1-\nu^2)}(I_1(\mathcal{E}) + 2\nu I_2(\mathcal{E})) + \frac{E}{(\nu+1)}I_3(\mathcal{E}). \tag{27}$$

where E and ν are the Young's modulus and Poisson ratio of the elastic sheet, respectively.

The mean and Gaussian curvatures can be expressed in terms of $w(\mathbf{x})$ as Abbena et al. (2006):

$$H = \nabla \cdot \left(\frac{\nabla w(\mathbf{x})}{\sqrt{1 + |\nabla w(\mathbf{x})|^2}}\right), \qquad K = \frac{\det(\nabla\nabla w(\mathbf{x}))}{(1 + |\nabla w(\mathbf{x})|^2)^2}. \tag{28}$$

Assuming small out-of-plane deformations, the expressions in (28) can be linearized as:

$$H = \nabla^2 w(\mathbf{x}), \quad K = \frac{\partial^2 w}{\partial x^2}\frac{\partial^2 w}{\partial y^2} - \left(\frac{\partial^2 w}{\partial x \partial y}\right)^2 \tag{29}$$

The elastic energy for the bending deformation of a membrane can be described as a quadratic function of the curvature field:

$$U_b = \int_S \left[\frac{1}{2}\kappa_b H^2 + \kappa_G K\right] dS, \tag{30}$$

where κ_b and κ_G are the bending and Gaussian moduli. In the remaining of this section we consider the periodic boundary conditions in all directions. The application of periodic boundary conditions ensures translational and rotational symmetries of all points on the surface, and also eliminates the effect of any edges. The absence of boundaries offers an additional advantage in facilitating the analytical procedure. The Gauss–Bonnet theorem (Abbena et al., 2006) states that the integral of the Gaussian curvature over a surface *without edges* remains invariant under any deformation that does not involve topological transformations. Thus, the contribution from the Gaussian curvature in Eq. (30) can be neglected for a membrane with periodic boundary conditions. Accordingly, the expression for the bending energy in its linearized form reduces to:

$$\begin{aligned} U_b &= \int \frac{1}{2}\kappa_b \left(\nabla^2 w\right)^2 = \int \frac{1}{2}\kappa_b \left(\nabla^2 (w_0(\mathbf{x}) + w'(\mathbf{x}))\right)^2 \\ &= \int \frac{1}{2}\kappa_b ((\nabla^2 w_0(\mathbf{x}))^2 + (\nabla^2 w'(\mathbf{x}))^2 + 2\nabla^2 w_0(\mathbf{x})\nabla^2 w'(\mathbf{x})). \end{aligned} \tag{31}$$

The total elastic energy of the sheet consists of contributions from both in-plane strain and out-of-plane bending. The complexity and anharmonicity of this energy arise primarily from two sources: (i) quartic terms involving the out-of-plane displacement field, and (ii) coupling terms between in-plane and out-of-plane displacements. In light of this, and following the framework of Ahmadpoor et al. (2017), we decompose the total elastic energy into three distinct parts: the harmonic energy U_{h}, the anharmonic coupling energy U_{ac} capturing interactions between in-plane and out-of-plane fields, and the purely anharmonic bending energy U_{anh} associated with higher-order out-of-plane contributions:

$$U = U_s + U_b = U_{\mathrm{h}} + U_{\mathrm{ac}} + U_{\mathrm{anh}}, \tag{32}$$

where each of the terms are expanded as below:

$$\begin{aligned} U_{\mathrm{h}} &= \frac{1}{2}\kappa_b \left(\nabla^2 w\right)^2 + \frac{E}{2(1-\nu^2)}\left(\left(\frac{\partial u_x}{\partial x}\right)^2 + \left(\frac{\partial u_y}{\partial y}\right)^2 + 2\nu\frac{\partial u_x}{\partial x}\frac{\partial u_y}{\partial y}\right) \\ &+ \frac{\varepsilon_0 E}{2(1-\nu^2)}\left(\nu\left(\frac{\partial w}{\partial x}\right)^2 + \left(\frac{\partial w}{\partial y}\right)^2\right) \\ &+ \frac{\varepsilon_0 E}{(1-\nu^2)}\left(\nu\frac{\partial u_x}{\partial x} + \frac{\partial u_y}{\partial y}\right) + \frac{E}{4(1+\nu)}\left(\frac{\partial u_x}{\partial y} + \frac{\partial u_y}{\partial x}\right)^2 + \frac{\varepsilon_0^2 E}{2(1-\nu^2)} \end{aligned} \tag{33a}$$

$$\begin{aligned} U_{\mathrm{ac}} &= \frac{E}{2(1-\nu^2)}\left(\frac{\partial u_x}{\partial x}\left(\frac{\partial w}{\partial x}\right)^2 + \frac{\partial u_y}{\partial y}\left(\frac{\partial w}{\partial y}\right)^2 + \nu\frac{\partial u_x}{\partial x}\left(\frac{\partial w}{\partial y}\right)^2 + \nu\frac{\partial u_y}{\partial y}\left(\frac{\partial w}{\partial x}\right)^2\right) \\ &+ \frac{E}{2(1+\nu)}\frac{\partial w}{\partial x}\frac{\partial w}{\partial y}\left(\frac{\partial u_x}{\partial y} + \frac{\partial u_y}{\partial x}\right) \end{aligned} \tag{33b}$$

$$U_{\mathrm{anh}} = \frac{E}{8(1-\nu^2)}\left(\left(\frac{\partial w}{\partial x}\right)^4 + \left(\frac{\partial w}{\partial y}\right)^4 + 2\left(\frac{\partial w}{\partial x}\frac{\partial w}{\partial y}\right)^2\right) \tag{33c}$$

To discretize the energy terms in Eq. (33) we use the Fourier expansion of the displacement field:

$$\begin{aligned} &\mathbf{u}(\mathbf{x}) = \sum_{\mathbf{q}\in\mathcal{K}} \overline{\mathbf{u}}(\mathbf{q})\mathbf{e}^{\imath\mathbf{q}\cdot\mathbf{x}}, \qquad w'(\mathbf{x}) = \sum_{\mathbf{q}\in\mathcal{K}} \overline{w}(\mathbf{q})\mathbf{e}^{\imath\mathbf{q}\cdot\mathbf{x}} \qquad w_0(\mathbf{x}) = \sum_{\mathbf{q}\in\mathcal{K}} \overline{w}_0(\mathbf{q})\mathbf{e}^{\imath\mathbf{q}\cdot\mathbf{x}} \\ &\frac{\partial w(\mathbf{x})}{\partial x_\gamma}\frac{\partial w(\mathbf{x})}{\partial x_\delta} = \sum_{\mathbf{q}\in\mathcal{K}} \overline{A}_{\gamma\delta}(\mathbf{q})\mathbf{e}^{\imath\mathbf{q}\cdot\mathbf{x}} \end{aligned} \tag{34}$$

where $\mathcal{K} := \{\mathbf{q} = 2\pi(\nu_x, \nu_y)/L : \nu_x, \nu_y \in \mathbb{Z}, |\mathbf{q}| \geqslant 2\pi/L\}$ and (γ, δ) denote (x, y). Also, $\mathbf{u}(\mathbf{x}) = (u_x(\mathbf{x}), u_y(\mathbf{x}))$.[3] The Fourier transforms of the displacement fields are:

$$\overline{\mathbf{u}}(\mathbf{q}) = \frac{1}{L^2}\int_{\mathbb{S}} \mathbf{u}(\mathbf{x})\mathbf{e}^{-\imath\mathbf{q}\cdot\mathbf{x}} d\mathbf{x}, \qquad \overline{w}(\mathbf{q}) = \frac{1}{L^2}\int_{\mathbb{S}} w(\mathbf{x})\mathbf{e}^{-\imath\mathbf{q}\cdot\mathbf{x}} d\mathbf{x} \tag{35}$$

$$\overline{A}_{\gamma\delta}(\mathbf{q}) = \frac{1}{L^2}\int_{\mathbb{S}} \frac{\partial w(\mathbf{x})}{\partial x_\gamma}\frac{\partial w(\mathbf{x})}{\partial x_\delta}\mathbf{e}^{-\imath\mathbf{q}\cdot\mathbf{x}} d\mathbf{x} \tag{36}$$

[3] Similarly, $\overline{\mathbf{u}}(\mathbf{q}) = (\overline{u}_x(\mathbf{q}), \overline{u}_y(\mathbf{q}))$.

The derivatives can be expressed in Fourier expansion as below:

$$\frac{\partial w(\mathbf{x})}{\partial x_\alpha}\frac{\partial w(\mathbf{x})}{\partial x_\beta} = \sum_{\mathbf{k}\in\mathcal{K}}\sum_{\mathbf{k}'\in\mathcal{K}} -k_\alpha k'_\beta \left(\overline{w}_0(\mathbf{k}) + \overline{w}'(\mathbf{k})\right)\left(\overline{w}_0(\mathbf{k}') + \overline{w}'(\mathbf{k}')\right)\mathbf{e}^{i(\mathbf{k}+\mathbf{k}')\cdot\mathbf{x}} = \sum_{\mathbf{q}\in\mathcal{K}} \overline{A}_{\alpha\beta}(\mathbf{q})\mathbf{e}^{i\mathbf{q}\cdot\mathbf{x}} \tag{37a}$$

In the expressions above, we have:

$$\mathbf{k}+\mathbf{k}' = \mathbf{q},$$
$$\overline{A}_{\alpha\beta}(\mathbf{q}) = \sum_{\mathbf{k}\in\mathcal{K}} -k_\alpha\left(q_\beta - k_\beta\right)\left(\overline{w}_0(\mathbf{k}) + \overline{w}'(\mathbf{k})\right)\left(\overline{w}_0(\mathbf{q}-\mathbf{k}) + \overline{w}'(\mathbf{q}-\mathbf{k})\right).$$

Further, the Fourier transform of the third order term capturing the coupling between in and out of plane displacement fields is:

$$\begin{aligned}\int_{\mathbb{S}}\left(\frac{\partial u_\gamma}{\partial x_\delta}\frac{\partial w}{\partial x_\alpha}\frac{\partial w}{\partial x_\beta}\right)d\mathbf{x} &= L^2\sum_{\mathbf{q}\in\mathcal{K}}\mathbf{i}\ q_\delta\overline{u}_\gamma(\mathbf{q})\overline{A}_{kl}(-\mathbf{q})\\ &= L^2\sum_{\mathbf{q}\in\mathcal{K}} q_\delta\Big\{\overline{A}^{\mathrm{Im}}_{kl}(\mathbf{q})\overline{u}^{\mathrm{Re}}_\gamma(\mathbf{q}) - \overline{u}^{\mathrm{Im}}_\gamma(\mathbf{q})\overline{A}^{\mathrm{Re}}_{kl}(\mathbf{q})\\ &\qquad + \mathbf{i}\left(\overline{A}^{\mathrm{Re}}_{kl}(\mathbf{q})\overline{u}^{\mathrm{Re}}_\gamma(\mathbf{q}) + \overline{u}^{\mathrm{Im}}_\gamma(\mathbf{q})\overline{A}^{\mathrm{Im}}_{kl}(\mathbf{q})\right)\Big\}\\ &= L^2\sum_{\mathbf{q}\in\mathcal{K}} q_\delta\left\{\overline{A}^{\mathrm{Im}}_{kl}(\mathbf{q})\overline{u}^{\mathrm{Re}}_\gamma(\mathbf{q}) - \overline{u}^{\mathrm{Im}}_\gamma(\mathbf{q})\overline{A}^{\mathrm{Re}}_{kl}(\mathbf{q})\right\}\end{aligned} \tag{38}$$

The superscripts "Re" and "Im" denote the decomposition into real and imaginary parts. Also note that we have dropped the imaginary part of the above summation, since it vanishes by summing over all modes.[4] Substituting the Fourier expansions in the expression for U_{h}, U_{ac}, and U_{anh}, yields the following:

$$\begin{aligned}\int U_{\mathrm{h}}d\mathbf{x} &= \frac{L^2}{2}\sum_{\mathbf{q}\in\mathcal{K}}\kappa_b\mathbf{q}^4|\overline{w}(\mathbf{q})|^2 + \frac{E}{1-\nu^2}\left(\mathbf{q}^2|\overline{\mathbf{u}}(\mathbf{q})|^2 + 2\nu q_x\overline{u}_x(\mathbf{q})q_y\overline{u}_y(\mathbf{q})\right)\\ &\quad + \frac{E}{1+\nu}\left(q_y^2|\overline{u}_x(\mathbf{q})|^2 + q_x^2|\overline{u}_y(\mathbf{q})|^2 - 2q_xq_y\overline{u}_x(\mathbf{q})\overline{u}_y(-\mathbf{q})\right)\\ &\quad + \frac{E\varepsilon_0}{2(1-\nu)}\mathbf{q}^2|\overline{w}(\mathbf{q})|^2 + \frac{E\varepsilon_0^2}{1-\nu}\\ &= \frac{L^2E\varepsilon_0^2}{2(1-\nu)} + \frac{L^2}{2}\sum_{\mathbf{q}\in\mathcal{K}}\overline{U}_{\mathrm{h}}(\mathbf{q})\end{aligned} \tag{39a}$$

$$\begin{aligned}\int U_{\mathrm{ac}}d\mathbf{x} &= \frac{L^2}{2}\sum_{\mathbf{q}\in\mathcal{K}}\frac{E}{1-\nu^2}\Big\{\overline{A}^{\mathrm{Re}}_{xx}(\mathbf{q})(q_x\overline{u}^{\mathrm{Im}}_x(\mathbf{q}) + \nu q_y\overline{u}^{\mathrm{Im}}_y(\mathbf{q})) + \overline{A}^{\mathrm{Re}}_{yy}(\mathbf{q})(q_y\overline{u}^{\mathrm{Im}}_y(\mathbf{q}) + \nu q_x\overline{u}^{\mathrm{Im}}_x(\mathbf{q}))\\ &\qquad - \overline{A}^{\mathrm{Im}}_{xx}(\mathbf{q})(q_x\overline{u}^{\mathrm{Re}}_x(\mathbf{q}) + \nu q_y\overline{u}^{\mathrm{Re}}_y(\mathbf{q})) - \overline{A}^{\mathrm{Im}}_{yy}(\mathbf{q})(q_y\overline{u}^{\mathrm{Re}}_y(\mathbf{q}) + \nu q_x\overline{u}^{\mathrm{Re}}_x(\mathbf{q}))\Big\}\\ &\quad + \frac{E}{1+\nu}\left\{\overline{A}^{\mathrm{Re}}_{xy}(\mathbf{q})(q_y\overline{u}^{\mathrm{Im}}_x(\mathbf{q}) + q_x\overline{u}^{\mathrm{Im}}_y(\mathbf{q})) - \overline{A}^{\mathrm{Im}}_{xy}(\mathbf{q})(q_y\overline{u}^{\mathrm{Re}}_x(\mathbf{q}) + q_x\overline{u}^{\mathrm{Re}}_y(\mathbf{q}))\right\}\\ &= \frac{L^2}{2}\sum_{\mathbf{q}\in\mathcal{K}}\overline{U}_{\mathrm{ac}}(\mathbf{q})\end{aligned} \tag{39b}$$

$$\begin{aligned}\int U_{\mathrm{anh}}d\mathbf{x} &= \frac{L^2}{8}\sum_{\mathbf{q}\in\mathcal{K}}\frac{E}{1-\nu^2}\left(|\overline{A}_{xx}(\mathbf{q})|^2 + |\overline{A}_{yy}(\mathbf{q})|^2 + 2|\overline{A}_{xy}(\mathbf{q})|^2\right)\\ &= \frac{L^2}{2}\sum_{\mathbf{q}\in\mathcal{K}}\overline{U}_{\mathrm{anh}}(\mathbf{q}).\end{aligned} \tag{39c}$$

[4] Note that for each $\mathbf{q}$ mode in the summation, there is a conjugate of $-\mathbf{q}$, that makes the imaginary part of the summation in (38) vanish:

$$\begin{aligned}&q_\delta\left(\overline{A}^{\mathrm{Re}}_{kl}(\mathbf{q})\overline{u}^{\mathrm{Re}}_\gamma(\mathbf{q}) + \overline{u}^{\mathrm{Im}}_\gamma(\mathbf{q})\overline{A}^{\mathrm{Im}}_{kl}(\mathbf{q})\right) + (-q_\delta)\left(\overline{A}^{\mathrm{Re}}_{kl}(-\mathbf{q})\overline{u}^{\mathrm{Re}}_\gamma(-\mathbf{q}) + \overline{u}^{\mathrm{Im}}_\gamma(-\mathbf{q})\overline{A}^{\mathrm{Im}}_{kl}(-\mathbf{q})\right)\\ &= q_\delta\left(\overline{A}^{\mathrm{Re}}_{kl}(\mathbf{q})\overline{u}^{\mathrm{Re}}_\gamma(\mathbf{q}) + \overline{u}^{\mathrm{Im}}_\gamma(\mathbf{q})\overline{A}^{\mathrm{Im}}_{kl}(\mathbf{q})\right) - q_\delta\left(\overline{A}^{\mathrm{Re}}_{kl}(\mathbf{q})\overline{u}^{\mathrm{Re}}_\gamma(\mathbf{q}) + (-\overline{u}^{\mathrm{Im}}_\gamma(\mathbf{q}))(-\overline{A}^{\mathrm{Im}}_{kl}(\mathbf{q}))\right)\\ &= 0\end{aligned}$$

.

We note that the total elastic energy is quadratic in the in-plane displacement field. This allows us to express the energy in Fourier space and subsequently perform the integration over the in-plane modes in the partition function:

$$\begin{aligned} Z &= \int \exp(-\beta U)\mathcal{D}[w,\mathbf{u}] \\ &= C(\varepsilon_0)\prod_{\mathbf{q}\in\mathcal{K}}\int_{-\infty}^{\infty}\exp\left(-\frac{\beta L^2}{2}\sum_{\mathbf{q}\in\mathcal{K}}(\overline{U}_{\mathrm{h}}(\mathbf{q})+\overline{U}_{\mathrm{ac}}(\mathbf{q})+\overline{U}_{\mathrm{anh}}(\mathbf{q}))\right) \\ &\qquad\qquad \times d\overline{w}(\mathbf{q})d\overline{u}_x^{\mathrm{Re}}(\mathbf{q})d\overline{u}_x^{\mathrm{Im}}(\mathbf{q})d\overline{u}_y^{\mathrm{Re}}(\mathbf{q})d\overline{u}_y^{\mathrm{Im}}(\mathbf{q}) \\ &= C(\varepsilon_0)\prod_{\mathbf{q}\in\mathcal{K}}\int \alpha(\mathbf{q})\exp(-\beta(U_b+U_s^{\mathrm{eff}}))d\overline{w}(\mathbf{q}) \end{aligned} \tag{40}$$

where $C(\varepsilon_0)=\exp(-\frac{\beta L^2 E\varepsilon_0^2}{2(1-\nu)})$ and $\alpha(\mathbf{q})=2(1-\nu)(1+\nu)^2\left(\frac{\pi k_B T}{EL^2|\mathbf{q}|^2}\right)^2$. Here, Gaussian integrals are used to integrate over the in-plane displacement components. As a result, the remaining terms in the exponent define an *effective strain energy* that depends only on the out-of-plane displacement field. The effective strain energy, that consists of the remainder terms once the in-plane terms have been integrated out, can be expressed as:

$$\begin{aligned} U_s^{\mathrm{eff}} &= \frac{E\varepsilon_0}{2(1-\nu)}L^2\sum_{\mathbf{q}\in\mathcal{K}}\left(\nu|k_x|^2+|k_y|^2\right)\left(|\overline{w}_0(\mathbf{k})|^2+|\overline{w}'(\mathbf{k})|^2+\overline{w}_0(\mathbf{k})\overline{w}'(-\mathbf{k})+\overline{w}_0(-\mathbf{k})\overline{w}'(\mathbf{k})\right) \\ &\quad+\frac{1}{8}EL^2\sum_{\mathbf{q}\in\mathcal{K}}\Psi(\mathbf{q})\Psi^*(\mathbf{q}), \end{aligned} \tag{41}$$

in which, for ease of notation, we have defined $\Psi(\mathbf{q})$ as:

$$\Psi(\mathbf{q})=\frac{1}{\mathbf{q}^2}\left\{q_y^2\overline{A}_{xx}(\mathbf{q})+q_x^2\overline{A}_{yy}(\mathbf{q})-2q_xq_y\overline{A}_{xy}(\mathbf{q})\right\}. \tag{42}$$

Furthermore, the strain energy can be compactly written using the transverse projector operator, as introduced in Nelson et al. (2004), as follows:

$$\Psi(\mathbf{q})=P_{ij}^T(\mathbf{q})\overline{A}_{ij}(\mathbf{q}), \tag{43}$$

in which

$$P_{ij}^T(\mathbf{q})=\delta_{ij}-\frac{q_iq_j}{\mathbf{q}^2}. \tag{44}$$

Accordingly, the total effective elastic energy in Fourier space can be written as:

$$\begin{aligned} U^{\mathrm{eff}} &= U_b+U_s^{\mathrm{eff}} \\ &= \frac{1}{2}\kappa_bL^2\sum_{\mathbf{k}\in\mathcal{K}}\mathbf{k}^4\left(|\overline{w}_0(\mathbf{k})|^2+|\overline{w}'(\mathbf{k})|^2+2\overline{w}_0(\mathbf{k})\overline{w}'(-\mathbf{k})\right) \\ &\quad+\frac{E\varepsilon_0}{2(1-\nu^2)}L^2\sum_{\mathbf{k}\in\mathcal{K}}\left(|\overline{w}_0(\mathbf{k})|^2+|\overline{w}'(\mathbf{k})|^2+\overline{w}_0(\mathbf{k})\overline{w}'(-\mathbf{k})+\overline{w}_0(-\mathbf{k})\overline{w}'(\mathbf{k})\right)(\nu k_x^2+k_y^2) \\ &\qquad+\frac{1}{2}EL^2\sum_{\mathbf{q}\in\mathcal{K}}\left|\frac{1}{2}P_{ij}^T(\mathbf{q})A_{ij}(\mathbf{q})\right|^2. \end{aligned} \tag{45}$$

To express the last term in Eq. (45) in terms of w_0 and w', we proceed as follow:

$$\begin{aligned} P_{ij}^T(\mathbf{q})\overline{A}_{ij}(\mathbf{q}) &= \sum_{\mathbf{k}\in\mathcal{K}}\left(-k_i(q_i-k_i)+\frac{k_iq_iq_j(q_j-k_j)}{\mathbf{q}^2}\right)\left(\overline{w}_0(\mathbf{k})+\overline{w}'(\mathbf{k})\right)\left(\overline{w}_0(\mathbf{q}-\mathbf{k})+\overline{w}'(\mathbf{q}-\mathbf{k})\right) \\ &= \sum_{\mathbf{k}\in\mathcal{K}}\frac{\mathbf{k}^2\mathbf{q}^2-(\mathbf{k}\cdot\mathbf{q})^2}{\mathbf{q}^2}\left(\overline{w}_0(\mathbf{k})+\overline{w}'(\mathbf{k})\right)\left(\overline{w}_0(\mathbf{q}-\mathbf{k})+\overline{w}'(\mathbf{q}-\mathbf{k})\right) \\ &= \sum_{\mathbf{k}\in\mathcal{K}}|\mathbf{k}|^2(\sin\theta_{\mathbf{q},\mathbf{k}})^2\left(\overline{w}_0(\mathbf{k})+\overline{w}'(\mathbf{k})\right)\left(\overline{w}_0(\mathbf{q}-\mathbf{k})+\overline{w}'(\mathbf{q}-\mathbf{k})\right), \end{aligned} \tag{46}$$

where, $\theta_{\mathbf{q},\mathbf{k}}$ is the angle between the vectors $\mathbf{q}$ and $\mathbf{k}$. The magnitude of the above expressions in each mode is then:

$$\begin{aligned} |P_{ij}^T(\mathbf{q})\overline{A}_{ij}(\mathbf{q})|^2 &= \left(P_{ij}^T(\mathbf{q})\overline{A}_{ij}(\mathbf{q})\right)\times\left(P_{ij}^T(-\mathbf{q})\overline{A}_{ij}(-\mathbf{q})\right) \\ &= \sum_{\mathbf{k},\mathbf{k}'\in\mathcal{K}}|\mathbf{k}|^2(\sin\theta_{\mathbf{q},\mathbf{k}})^2|\mathbf{k}'|^2(\sin\theta_{-\mathbf{q},\mathbf{k}'})^2\left(\overline{w}_0(\mathbf{k})+\overline{w}'(\mathbf{k})\right)\left(\overline{w}_0(\mathbf{q}-\mathbf{k})+\overline{w}'(\mathbf{q}-\mathbf{k})\right) \\ &\qquad\times\left(\overline{w}_0(\mathbf{k}')+\overline{w}'(\mathbf{k}')\right)\left(\overline{w}_0(-\mathbf{q}-\mathbf{k}')+\overline{w}'(-\mathbf{q}-\mathbf{k}')\right). \end{aligned} \tag{47}$$

Up to this point, the derivation has effectively decoupled the in-plane and out-of-plane displacements. We are now left with a nonlinear statistical mechanics problem governed by the effective energy U^{eff}, which depends solely on the out-of-plane displacement

w. The onset of buckling in a thermally fluctuating elastic sheet can be characterized by examining the fluctuation spectrum. As the compressive strain approaches its critical value, fluctuations about the flat configuration grow unbounded, indicating a transition to a new stable, buckled state. To analyze the fluctuation spectrum within the nonlinear energy framework of Eq. (45), we follow the approach of Ahmadpoor et al. (2017) and apply variational perturbation theory to obtain an approximate expression for the fluctuations spectrum. We start with the trial quadratic energy function as below:

$$\mathcal{H}_{\text{trial}} = \frac{1}{2}L^2 \sum_{\mathbf{k}\in\mathcal{K}} \kappa^{\text{eff}}(\mathbf{k})|\mathbf{k}|^4 |w'(\mathbf{k})|^2 \tag{48}$$

where $\kappa^{\text{eff}}(\mathbf{k})$ is the unknown mode dependent effective bending stiffness. The variational free energy up to Mth order is then expanded as:

$$F_M = F_0 - \frac{1}{\beta}\sum_{N=1}^{M} \frac{(-\beta)^N}{N!} \langle \left[U_b + U_s^{\text{eff}} - \mathcal{H}_{\text{trial}}\right]^N \rangle^c_{\mathcal{H}_{\text{trial}}} \tag{49}$$

where F_0 is the free energy corresponding to the trial energy $\mathcal{H}_{\text{trial}}$:

$$F_0 = \sum_{\mathbf{k}\in\mathcal{K}} \frac{1}{2\beta}\left(\log(\frac{L^2|\mathbf{k}|^4}{2\pi}) + \log(\beta\kappa^{\text{eff}}(\mathbf{k}))\right) = C_F + \sum_{\mathbf{k}\in\mathcal{K}} \frac{1}{2\beta}\log(\beta\kappa^{\text{eff}}(\mathbf{k})) \tag{50}$$

where C_F, is coefficient, independent of the effective stiffness $\kappa^{\text{eff}}(\mathbf{k})$. The full expansion in Eq. (A.8), as $N \to \infty$, is independent of the choice of the trial energy function. In practice, however, the series is truncated at a finite order M to estimate the free energy. Unlike the full expansion, the truncated series F_M generally depends on the specific form of the trial energy function $\mathcal{H}_{\text{trial}}$. To obtain an optimized estimate, we therefore minimize the *sensitivity* of F_M to variations in $\mathcal{H}_{\text{trial}}$, following the procedure in Ahmadpoor et al. (2017):

$$\frac{\partial F_M}{\partial \kappa^{\text{eff}}(\mathbf{k})} := 0. \tag{51}$$

In what follows, we will use this approach up to first order to obtain a closed form estimation of the effective stiffness of the system which will be used to analyze the buckling threshold for the membrane in the presence of both imperfection field and thermal fluctuations. We proceed to calculate the expectation values in the right hand side of Eq. (A.8) up to first order with respect to the trial quadratic energy $\mathcal{H}_{\text{trial}}$. In the following we will use the equipartition theorem (Kittel, 2004) as well as Wick's theorem (Kleinert, 1989) to calculate the ensemble averages as follows:

$$\begin{aligned}
&\langle |\overline{w}'(\mathbf{k})|^2 \rangle_{\mathcal{H}_{\text{trial}}} = \frac{k_B T}{L^2|\mathbf{k}|^4\kappa^{\text{eff}}(\mathbf{k})} \\
&\langle \overline{w}'(\mathbf{k}_1)\overline{w}'(\mathbf{k}_2)\overline{w}'(\mathbf{k}_3)\overline{w}'(\mathbf{k}_4)\rangle_{\mathcal{H}_{\text{trial}}} = \langle |\overline{w}'(\mathbf{k}_1)|^2 \rangle_{\mathcal{H}_{\text{trial}}} \langle |\overline{w}'(\mathbf{k}_2)|^2 \rangle_{\mathcal{H}_{\text{trial}}} \Big\{ \delta(\mathbf{k}_1,-\mathbf{k}_3)\delta(\mathbf{k}_2,-\mathbf{k}_4) \\
&\qquad + \delta(\mathbf{k}_1,-\mathbf{k}_4)\delta(\mathbf{k}_2,-\mathbf{k}_3) \Big\} + \langle |\overline{w}'(\mathbf{k}_1)|^2 \rangle_{\mathcal{H}_{\text{trial}}} \langle |\overline{w}'(\mathbf{k}_3)|^2 \rangle_{\mathcal{H}_{\text{trial}}} \delta(\mathbf{k}_1,-\mathbf{k}_2)\delta(\mathbf{k}_3,-\mathbf{k}_4).
\end{aligned} \tag{52}$$

Substituting the ensemble averages above in the first order variational free energy in (A.8) we have:

$$\begin{aligned}
F_{\text{var}} &= F_0 + \langle U_b \rangle_{\mathcal{H}_{\text{trial}}} + \langle U_s^{\text{eff}} \rangle_{\mathcal{H}_{\text{trial}}} = C_F + \sum_{\mathbf{k}\in\mathcal{K}} \frac{1}{2}k_B T \log(\kappa^{\text{eff}}(\mathbf{k})) \\
&+ \frac{1}{2}L^2 \sum_{\mathbf{k}\in\mathcal{K}} \left(\kappa_b \mathbf{k}^4 + \frac{E\varepsilon_0}{1-\nu^2}\left(\nu\mathbf{k}_x^2 + \mathbf{k}_y^2\right)\right)\left(|\overline{w}_0(\mathbf{k})|^2 + \langle |\overline{w}'(\mathbf{k})|^2 \rangle_{\mathcal{H}_{\text{trial}}}\right) \\
&+ \frac{1}{2}EL^2 \sum_{\mathbf{q}\in\mathcal{K}} \langle |\frac{1}{2}P_{ij}^T(\mathbf{q})\overline{A}_{ij}(\mathbf{q})|^2 \rangle_{\mathcal{H}_{\text{trial}}} = C_F + \sum_{\mathbf{k}\in\mathcal{K}} \frac{1}{2}k_B T \log(\kappa^{\text{eff}}(\mathbf{k})) \\
&+ \frac{1}{2}L^2 \sum_{\mathbf{k}\in\mathcal{K}} \left(\kappa_b|\mathbf{k}|^4 + \frac{E\varepsilon_0}{1-\nu^2}\left(\nu\mathbf{k}_x^2 + \mathbf{k}_y^2\right)\right)\left(|\overline{w}_0(\mathbf{k})|^2 + \frac{1}{L^2\beta\kappa^{\text{eff}}(\mathbf{k})|\mathbf{k}|^4}\right) \\
&+ \frac{1}{2}EL^2 \sum_{\mathbf{q},\mathbf{k},\mathbf{k}'\in\mathcal{K}} |\mathbf{k}|^2(\sin\theta_{\mathbf{q},\mathbf{k}})^2|\mathbf{k}'|^2(\sin\theta_{-\mathbf{q},\mathbf{k}'})^2 \overline{w}_0(\mathbf{k})\overline{w}_0(\mathbf{q}-\mathbf{k})\overline{w}_0(\mathbf{k}')\overline{w}_0(-\mathbf{q}-\mathbf{k}') \\
&+ \frac{1}{2}EL^2 \sum_{\mathbf{q},\mathbf{k}\in\mathcal{K}} |\mathbf{k}|^4(\sin\theta_{\mathbf{q},\mathbf{k}})^4 \Bigg\{ \frac{|\overline{w}_0(\mathbf{q}-\mathbf{k})|^2 + |\overline{w}_0(\mathbf{k})|^2}{L^2\beta\kappa^{\text{eff}}(\mathbf{k})|\mathbf{k}|^4} + \frac{|\overline{w}_0(\mathbf{k})|^2 + |\overline{w}_0(\mathbf{q}-\mathbf{k})|^2}{L^2\beta\kappa^{\text{eff}}(\mathbf{q}-\mathbf{k})|\mathbf{q}-\mathbf{k}|^4} \\
&+ \frac{2}{\left(L^2\beta\kappa^{\text{eff}}(\mathbf{k})|\mathbf{k}|^4\right)\left(L^2\beta\kappa^{\text{eff}}(\mathbf{q}-\mathbf{k})|\mathbf{q}-\mathbf{k}|^4\right)} \Bigg\}
\end{aligned} \tag{53}$$

Minimizing the sensitivity of the variational free energy in (53) with respect to the trial energy function parameter $\kappa^{\text{eff}}(\mathbf{k})$, we set:

$$\frac{\partial F_{var}}{\partial \kappa^{\text{eff}}(\mathbf{k})} := 0 = \sum_{\mathbf{k}\in\mathcal{K}} \Bigg\{ \frac{1}{2\beta\kappa^{\text{eff}}(\mathbf{k})} - \frac{\kappa_b}{2\beta\kappa^{\text{eff}}(\mathbf{k})^2} - \frac{E\varepsilon_0\left(\nu|k_x|^2+|k_y|^2\right)}{2\beta(1-\nu^2)\kappa^{\text{eff}}(\mathbf{k})^2|\mathbf{k}|^4}$$
$$- \frac{EL^2}{2}\sum_{\mathbf{q}\in\mathcal{K}}|\mathbf{k}|^4(\sin\theta_{\mathbf{q},\mathbf{k}})^4\Bigg\{\frac{\left(|\overline{w}_0(\mathbf{k})|^2+|\overline{w}_0(\mathbf{q}-\mathbf{k})|^2\right)}{L^2\beta|\mathbf{q}-\mathbf{k}|^4}\left(\frac{|\mathbf{k}|}{\kappa^{\text{eff}}(\mathbf{q}-\mathbf{k})\kappa^{\text{eff}}(\mathbf{k})|\mathbf{q}-\mathbf{k}|}\right)$$
$$+ \frac{\left(|\overline{w}_0(\mathbf{k})|^2+|\overline{w}_0(\mathbf{q}-\mathbf{k})|^2\right)}{L^2\beta\kappa^{\text{eff}}(\mathbf{k})^2|\mathbf{k}|^4} + \frac{2}{L^4\beta^2|\mathbf{k}|^4|\mathbf{q}-\mathbf{k}|^4\kappa^{\text{eff}}(\mathbf{k})^2\kappa^{\text{eff}}(\mathbf{q}-\mathbf{k})}\left(1+\frac{|\mathbf{k}|}{|\mathbf{q}-\mathbf{k}|}\right)\Bigg\}\Bigg\},$$

from which the implicit equation for the effective bending stiffness $\kappa^{\text{eff}}(\mathbf{k})$ is obtained as:

$$\kappa^{\text{eff}}(\mathbf{k}) = \kappa_b + \frac{E\varepsilon_0\left(\nu|k_x|^2+|k_y|^2\right)}{(1-\nu^2)|\mathbf{k}|^4}$$
$$+ E\sum_{\mathbf{q}\in\mathcal{K}}(\sin\theta_{\mathbf{q},\mathbf{k}})^4\Bigg\{\left(|\overline{w}_0(\mathbf{k})|^2+|\overline{w}_0(\mathbf{q}-\mathbf{k})|^2\right)\left(1+\frac{|\mathbf{k}|^5\kappa^{\text{eff}}(\mathbf{k})}{|\mathbf{q}-\mathbf{k}|^5\kappa^{\text{eff}}(\mathbf{q}-\mathbf{k})}\right)$$
$$+ \frac{2k_BT}{L^2|\mathbf{q}-\mathbf{k}|^4\kappa^{\text{eff}}(\mathbf{q}-\mathbf{k})}\left(1+\frac{|\mathbf{k}|}{|\mathbf{q}-\mathbf{k}|}\right)\Bigg\}$$
$$= \kappa_b + \frac{E\varepsilon_0\left(\nu|k_x|^2+|k_y|^2\right)}{(1-\nu^2)|\mathbf{k}|^4}$$
$$+ E\sum_{\mathbf{q}\in\mathcal{K}}(\sin\theta_{\mathbf{q},\mathbf{k}})^4\Bigg\{\left(|\overline{w}_0(\mathbf{k})|^2+|\overline{w}_0(\mathbf{q}-\mathbf{k})|^2\right)\left(1+\frac{|\mathbf{k}|\langle|\overline{w}'(\mathbf{q}-\mathbf{k})|^2\rangle}{|\mathbf{q}-\mathbf{k}|\langle|\overline{w}'(\mathbf{k})|^2\rangle}\right)$$
$$+ 2\langle|\overline{w}'(\mathbf{q}-\mathbf{k})|^2\rangle\left(1+\frac{|\mathbf{k}|}{|\mathbf{q}-\mathbf{k}|}\right)\Bigg\}, \tag{54}$$

where we used the fluctuations spectra equations for modes $\mathbf{k}$ and $\mathbf{q}-\mathbf{k}$ to further simplify the expression for the effective bending stiffness. The above expression, in the absence of a preexisting field w_0, was previously derived by Ahmadpoor et al. (2017). Prior to studying the buckling behavior, we revisit the effective bending stiffness of a fluctuating sheet with and without imperfection.

- **Effective stiffness of a fluctuating sheet without imperfection:** In this case that has been previously studied in Ahmadpoor et al. (2017), $w_0 = 0$ as well as $\varepsilon_0 = 0$, and thus the (54) reduces to:

$$\kappa^{\text{eff}}(\mathbf{k}) = \kappa_b + \sum_{\mathbf{q}\in\mathcal{K}}\frac{2Ek_BT(\sin\theta_{\mathbf{q},\mathbf{k}})^4}{L^2|\mathbf{q}-\mathbf{k}|^4\kappa^{\text{eff}}(\mathbf{q}-\mathbf{k})}\left(1+\frac{|\mathbf{k}|}{|\mathbf{q}-\mathbf{k}|}\right) \tag{55}$$

  Following Ahmadpoor et al. (2017), we focus on the long-wavelength limit ($|\mathbf{q}|, |\mathbf{k}|) \to 0$, as these modes dominate the fluctuation spectrum. To enable analytical progress, we approximate the effective bending rigidity as $\kappa^{\text{eff}}(\mathbf{q}-\mathbf{k}) \sim \Theta|\mathbf{q}-\mathbf{k}|^{-\zeta}$, where Θ is an undetermined constant. Under this approximation, the summation in the second term of Eq. (55) scales as:

$$\sum_{\mathbf{q}\in\mathcal{K}}\frac{Ek_BT(\sin\theta_{\mathbf{q},\mathbf{k}})^4}{L^2|\mathbf{q}-\mathbf{k}|^4\kappa^{\text{eff}}(\mathbf{q}-\mathbf{k})}\left(1+\frac{|\mathbf{k}|}{|\mathbf{q}-\mathbf{k}|}\right) \sim \sum_{\mathbf{q}\in\mathcal{K}}\frac{Ek_BT}{L^2\Theta|\mathbf{q}-\mathbf{k}|^{4-\zeta}}\left(1+\frac{|\mathbf{k}|}{|\mathbf{q}-\mathbf{k}|}\right)$$
$$\sim \frac{Ek_BT}{\Theta|\mathbf{k}|^{2-\zeta}}.$$

  At long wavelengths, the summation in Eq. (55) dominates over the constant term κ_b in Eq. (55). As a result, the effective bending stiffness for long-wavelength fluctuations scales as

$$\kappa^{\text{eff}}(\mathbf{k}) := \Theta|\mathbf{k}|^{-\zeta} \sim \frac{k_BTE}{\Theta|\mathbf{k}|^{2-\zeta}}. \tag{56}$$

  Solving for $\kappa^{\text{eff}}(\mathbf{k})$ yields the scaling relation:

$$\kappa^{\text{eff}}(\mathbf{k}) \sim \sqrt{Ek_BT}\,|\mathbf{k}|^{-1}. \tag{57}$$

- **Effective stiffness of a nonlinear elastic sheet with imperfection at zero Kelvin:** In this case, we assume the sheet is at zero Kelvin, with no thermal fluctuations. This effectively eliminates the last term in Eq. (54), reducing the effective bending stiffness in the absence of both external strain and thermal fluctuations to:

$$\kappa^{\text{eff}}(\mathbf{k}) = \kappa_b + E\sum_{\mathbf{q}\in\mathcal{K}}(\sin\theta_{\mathbf{q},\mathbf{k}})^4\Bigg\{\left(|\overline{w}_0(\mathbf{k})|^2+|\overline{w}_0(\mathbf{q}-\mathbf{k})|^2\right)\left(1+\frac{|\mathbf{k}|^5\kappa^{\text{eff}}(\mathbf{k})}{|\mathbf{q}-\mathbf{k}|^5\kappa^{\text{eff}}(\mathbf{q}-\mathbf{k})}\right)\Bigg\}$$
$$\sim \kappa_b + c_1E|\overline{w}_0|^2, \tag{58}$$

  where c_1 is simply a coefficient after calculating the summation over $\mathbf{q}$.

It is instructive to compare the effective bending stiffness with that of a classical plate characterized by (the bulk or 3D) Young's modulus Y and thickness t, where the bending rigidity scales as $D \sim Yt^3$. In contrast, for crystalline membranes considered in

this work, the bending modulus κ_b is an independent material property. Additionally, the relevant in-plane stiffness is the two-dimensional Young's modulus, defined as $E = Yt$, where Y is the bulk modulus. Under this relation, the bending stiffness of an equivalent classical plate becomes $D \sim Et^2$. When imperfections or preexisting out-of-plane displacements are present, their amplitude effectively serves as a thickness scale. As a result, the effective bending stiffness varies with the preexisting wrinkling amplitude as $\kappa^{\text{eff}} \sim E|w_0|^2$. Similarly, looking at the last term in Eq. (54), the effective bending stiffness also varies with the amplitude of the thermal fluctuations as $\kappa^{\text{eff}} \sim E\langle w'^2\rangle$, where the mean square root of the thermal fluctuations serves as the effective thickness of the equivalent plate. While the combined effect of imperfection field and thermal fluctuations is a nonlinear problem to solve for the effective bending stiffness, within a first order approximation one can write:

$$\kappa^{\text{eff}}(\mathbf{k}) = c_1 E|\overline{w}_0|^2 + c_2\sqrt{Ek_BT}|\mathbf{k}|^{-1}. \tag{59}$$

In the following, we incorporate the compressive strain term into the effective bending stiffness and determine the critical compressive strain at which the effective stiffness vanishes, signaling the onset of buckling.

- **Critical buckling strain of a nonlinear elastic sheet with imperfection at zero Kelvin:** In this case, we assume the sheet is at zero Kelvin, with no thermal fluctuations. The buckling occurs when the effective bending stiffness in Eq. (54) vanishes. Considering the buckling of first few modes, where $|\mathbf{k}|$ is small, the critical strain scales with the imperfection amplitude as:

$$\kappa^{\text{eff}}(\mathbf{k}) \sim \frac{E\varepsilon_0}{|\mathbf{k}|^2} + c_1 E|\overline{w}_0|^2 := 0, \quad \rightarrow \quad \varepsilon^{cr}(\mathbf{k}) \sim |\mathbf{k}|^2|\overline{w}_0|^2, \tag{60}$$

  from which the critical strain for the first mode (where $|\mathbf{k}| = 2\pi/L$) buckling scales as: $\varepsilon^{cr} \propto \frac{|\overline{w}_0|^2}{L^2}$.
- **Critical buckling strain of a nonlinear elastic sheet without imperfection at finite temperature:** In this scenario, the sheet is assumed to be perfectly flat and free of imperfections at zero Kelvin. At finite temperatures, however, thermal fluctuations arise, influencing the buckling threshold relative to the zero-temperature case. To determine how the critical buckling strain scales with the system size (or mode ($\mathbf{k}$)), we set the effective bending stiffness to zero:

$$\kappa^{\text{eff}}(\mathbf{k}) \sim \frac{E\varepsilon_0}{|\mathbf{k}|^2} + c_2 E\langle w'^2\rangle := 0, \quad \rightarrow \quad \varepsilon^{cr}(\mathbf{k}) \sim \langle w'^2\rangle|\mathbf{k}|^2 \tag{61}$$

  from which the critical strain for the first mode (where $|\mathbf{k}| = 2\pi/L$) buckling scales as: $\varepsilon^{cr} \propto \frac{\langle w'^2\rangle}{L^2}$. Since the fluctuations amplitude also scales with the planar size of the membrane and temperature as $\langle w'^2\rangle \propto L^{2-\zeta}T^{\delta}$, where ζ and δ are obtained to be $\zeta = 1$ and $\delta = 0.5$ using the VPT in Eq. (57), the critical strain also scales with length L and temperature T as: $\varepsilon^{cr} \propto L^{-\zeta} \propto \sqrt{T}L^{-1}$.

As demonstrated by our analysis, the buckling threshold is influenced by both structural imperfections and thermal fluctuations. The out-of-plane deformations induced by defects and imperfections are typically on the order of interatomic distances, usually a few angstroms, and remain largely independent of temperature and system size. In contrast, the amplitude of thermally induced fluctuations depends strongly on both the lateral dimension of the membrane L and the ambient temperature T. For example, in membranes with lateral dimensions of a few hundred nanometers, the root-mean-square amplitude of thermal undulations at room temperature can reach approximately one nanometer, making them comparable in magnitude to typical geometric imperfections. At higher temperatures and for larger membranes, thermal fluctuations become significantly more pronounced — often exceeding the amplitude of the imperfections by an order of magnitude. As a result, in this regime, the buckling behavior becomes dominated by entropic effects, and the system exhibits reduced sensitivity to imperfections. This size- and temperature-dependent crossover highlights the need to account for thermal fluctuations when assessing the mechanical stability of flexible membranes, particularly in nanoscale and high-temperature applications.

We note that the effective bending stiffness and the critical buckling load of a perfect sheet have previously been derived using variational perturbation theory (VPT) (Ahmadpoor et al., 2017) and renormalization group (RG) theory (Morshedifard et al., 2021; Košmrlj and Nelson, 2016). However, a slight discrepancy exists between the two approaches in the predicted value of the exponent ζ, which may arise from differences in material properties or the underlying computational and analytical techniques.

4. Summary and conclusion

The stability or instability of thermally fluctuating filaments and membranes has important implications across both biological systems and nanoscale engineering. In cellular biology, the controlled buckling of cytoskeletal filaments such as actin and microtubules enables force transmission, shape regulation, and mechanosensitive responses essential to cell motility, division, and morphogenesis. Thermal softening and fluctuation-assisted buckling play critical roles in processes like lamellipodial extension, endocytosis, and the generation of intracellular protrusions. In nanotechnology, buckling instabilities are increasingly exploited in the design of responsive and reconfigurable nanostructures, including kirigami-based devices, stretchable electronics, and drug delivery capsules. The ability to tune buckling thresholds through temperature, geometry, or controlled imperfections provides a powerful mechanism for achieving adaptive functionality in flexible 2D materials and polymer-based systems. Understanding the interplay between thermal fluctuations and mechanical instability is therefore essential for both predicting failure and harnessing structural transitions in soft, low-dimensional systems. This work presents a theoretical framework for analyzing the buckling behavior of thermally fluctuating rods and crystalline membranes, incorporating the effects of thermal fluctuations, geometric

nonlinearities, and structural imperfections. By formulating statistical mechanical models that explicitly account for entropy-driven deformation modes, we provide insight into how these effects jointly govern the mechanical stability of low-dimensional elastic systems.

At low temperatures, where thermal fluctuations are negligible, the buckling behavior of slender rods and sheets closely follows classical predictions based on ground-state elasticity. In this regime, the critical buckling force and post-buckling configuration are well described by elasticity theory. Similarly, for filaments with small L/l_p ratios, where L is the contour length and l_p the persistence length, fluctuations are suppressed, and the filament behaves as a rigid bar, displaying a sharp buckling transition akin to its zero-temperature counterpart.

In contrast, soft filaments and systems with large L/l_p ratios enter a thermally dominated regime in which fluctuations significantly alter mechanical response. Under these conditions, the buckling transition becomes smooth and gradual, reflecting the role of thermal undulations in softening the effective stiffness. These effects are especially pronounced in flexible biopolymers, where entropic forces shape the force–extension behavior even below the classical buckling threshold.

For crystalline membranes, both thermal fluctuations and imperfections influence the onset of buckling. The amplitude of imperfections, typically on the order of angstroms, can be comparable to the amplitude of thermal fluctuations for sheets with lateral dimensions of a few hundred nanometers at room temperature. However, at higher temperatures or for larger membranes, the amplitude of thermal fluctuations can exceed that of the imperfections by an order of magnitude or more, effectively suppressing the membrane's sensitivity to defects. Given the approximate nature of the analytical approach used in this work, we have focused on two distinct regimes: (i) a perfect sheet influenced solely by thermal fluctuations, and (ii) a defected sheet exhibiting static wrinkles in the absence of thermal fluctuations. Obtaining accurate quantitative predictions, however, requires computational tools capable of handling large system sizes and long time scales in order to capture the coupled effects of defects and thermal fluctuations.

The problems studied in this paper are inherently nonlinear due to the large deformations and geometric nonlinearities. To implement these nonlinearities within the statistical mechanics framework, we employed the variational perturbation theory (VPT) (Ahmadpoor et al., 2017), which allows for an approximate but self-consistent treatment of fluctuation-induced renormalizations. Our analysis reveals that, in the absence of imperfections, thermal fluctuations alone significantly modify the scaling law for the critical buckling strain. While at zero Kelvin the critical strain follows the classical length scaling $\varepsilon_0^{cr} \propto 1/L^2$, our VPT-based calculations show that at finite temperature the scaling law becomes $\varepsilon_T^{cr} \propto \sqrt{T}/L$. This result highlights the importance of incorporating temperature-dependent entropic effects in predicting the stability of thermally fluctuating membranes.

Overall, our findings demonstrate that the mechanical stability of low-dimensional structures is not a purely deterministic property but is critically influenced by fluctuations and defects. Importantly, imperfection sensitivity in such systems is scale- and temperature-dependent, which has direct implications for the design and reliability of nanoscale materials and devices. Although the problem under investigation presents significant mathematical and experimental challenges, our qualitative findings mark an initial step toward understanding the role of entropic effects in the stability of flexible nanostructures. These results highlight the need for continued development of both computational models and experimental approaches that can systematically incorporate entropic contributions into the study of the mechanics of flexible nanostructures. Future work could extend this framework to include time-dependent phenomena, active fluctuations in biological systems, or coupling with substrate and environmental constraints. Such extensions would provide a more comprehensive understanding of entropy-driven instabilities in soft and flexible nanostructures.

CRediT authorship contribution statement

Xin Yan: Writing – review & editing, Writing – original draft, Methodology, Investigation, Formal analysis. **Md Sojib Kaisar:** Validation, Methodology, Formal analysis. **Rubayet Hassan:** Validation, Formal analysis. **Fatemeh Ahmadpoor:** Writing – review & editing, Writing – original draft, Supervision, Project administration, Funding acquisition, Conceptualization.

Declaration of competing interest

The authors declare the following financial interests/personal relationships which may be considered as potential competing interests: Fatemeh Ahmadpoor reports financial support was provided by National Science Foundation. If there are other authors, they declare that they have no known competing financial interests or personal relationships that could have appeared to influence the work reported in this paper.

Acknowledgments

Fatemeh Ahmadpoor gratefully acknowledge financial support from the New Jersey Institute of Technology and the National Science Foundation, United States through Grant No. CMMI-2237530.

Appendix. The variational perturbation theory

Consider a nonlinear energy function $\mathcal{H} = \mathcal{H}_0 + \mathcal{H}_p$. Suppose that the nonlinear part $\mathcal{H}_p$ is a small perturbation compared to the quadratic functional $\mathcal{H}_0$. Let F, be the free energy of the system. In the absence of the nonlinear perturbation term $\mathcal{H}_p$, the partition function Z_0 and free energy F_0 can be easily obtained using standard Gaussian integrations. The effect of the nonlinear term on the total free energy of the system can be then estimated by a perturbation expansion around F_0. We start with expanding the partition function of the system Z:

$$Z = \int \exp(-\beta(\mathcal{H}_0 + \mathcal{H}_p))\mathcal{D}[w] = Z_0\langle \exp(-\beta\mathcal{H}_p)\rangle_{\mathcal{H}_0} \tag{A.1}$$

wherein $\beta = \frac{1}{k_B T}$ and the subscript $\langle\cdot\rangle_{\mathcal{H}_0}$ denotes ensemble average, with respect to $\mathcal{H}_0$. The exponential term in the above equation can be expanded in a Taylor series as:

$$\exp(-\beta\mathcal{H}_p) = 1 - \beta\mathcal{H}_p + \frac{1}{2}(\beta\mathcal{H}_p)^2 + \cdots = \sum_{n=0}^{\infty} \frac{(-\beta\mathcal{H}_p)^n}{n!} \tag{A.2}$$

Then the free energy of the system is obtained as:

$$F = -\frac{1}{\beta}\log Z = F_0 - \frac{1}{\beta}\log(1 + \sum_{n=1}^{\infty} \frac{\langle(-\beta\mathcal{H}_p)^n\rangle_{\mathcal{H}_0}}{n!}) \tag{A.3}$$

Expanding the logarithm term we have:

$$\log\left(\sum_{n=0}^{\infty} \frac{(-\beta)^n\langle\mathcal{H}_p^n\rangle_{\mathcal{H}_0}}{n!}\right) = \left(\sum_{n=1}^{\infty} \frac{(-\beta)^n\langle\mathcal{H}_p^n\rangle_{\mathcal{H}_0}}{n!}\right) - \frac{1}{2}\left(\sum_{n=1} \frac{(-\beta)^n\langle\mathcal{H}_p^n\rangle_{\mathcal{H}_0}}{n!}\right)^2 + \cdots \tag{A.4}$$

and hence, the free energy expansion can be derived to be:

$$F = F_0 - \frac{1}{\beta}\sum_{n=1}^{\infty} \frac{(-\beta)^n}{n!}\langle\mathcal{H}_p^n\rangle^c_{\mathcal{H}_0} \tag{A.5}$$

where the superscript $\langle\cdot\rangle^c$ denotes the cumulant averages. The cumulant averages, up to fourth order, are:

$$\begin{aligned}
&\langle\mathcal{H}_p\rangle^c_{\mathcal{H}_0} = \langle\mathcal{H}_p\rangle_{\mathcal{H}_0}\\
&\langle\mathcal{H}_p^2\rangle^c_{\mathcal{H}_0} = \langle\mathcal{H}_p^2\rangle_{\mathcal{H}_0} - \langle\mathcal{H}_p\rangle^2_{\mathcal{H}_0}\\
&\langle\mathcal{H}_p^3\rangle^c_{\mathcal{H}_0} = \langle\mathcal{H}_p^3\rangle_{\mathcal{H}_0} - 3\langle\mathcal{H}_p^2\rangle_{\mathcal{H}_0}\langle\mathcal{H}_p\rangle_{\mathcal{H}_0} + 2\langle\mathcal{H}_p\rangle^3_{\mathcal{H}_0}\\
&\langle\mathcal{H}_p^4\rangle^c_{\mathcal{H}_0} = \langle\mathcal{H}_p^4\rangle_{\mathcal{H}_0} - 3\langle\mathcal{H}_p^3\rangle_{\mathcal{H}_0}\langle\mathcal{H}_p\rangle_{\mathcal{H}_0} - 3\langle\mathcal{H}_p^2\rangle^2_{\mathcal{H}_0} + 12\langle\mathcal{H}_p^2\rangle_{\mathcal{H}_0}\langle\mathcal{H}_p\rangle^2_{\mathcal{H}_0} - 6\langle\mathcal{H}_p\rangle^4_{\mathcal{H}_0}
\end{aligned}$$

Accordingly, the excess free energy can be related to the total average energy of the system up to nth order as:

$$\langle\mathcal{H}\rangle = \langle\mathcal{H}_0\rangle_{\mathcal{H}_0} + \frac{1}{\beta}\sum_{n=1}^{\infty} \frac{(-\beta)^n}{n!}\langle\mathcal{H}_p^n\rangle^c_{\mathcal{H}_0}$$

The infinite series in the above equation gives us the exact average amount of energy that the nonlinear term adds to the system. In practice, however, we need to truncate the series to some finite order. If the nonlinear term is small (and the series is well-behaved), we can expect to achieve a reasonable estimate by evaluating the first few terms of perturbation expansion in Eq. (A.5). Yet, it has been shown that the effect of nonlinearities in solid membranes such as graphene is indeed remarkable and the naive perturbation method does not provide a reasonable estimate for the free energy and fluctuations (Ahmadpoor et al., 2017).

To improve the results of what can be obtained from the naive perturbation approach, we adopt an alternative version of it that is rooted in a variational argument. The key idea was first introduced by Kleinert (2009) in the context of anharmonic Hamiltonians arising in quantum mechanics. We briefly elaborate on the details of the procedure here. We start with adding and subtracting a trial Hamiltonian to the nonlinear energy formulation. Consider a trial Hamiltonian as:

$$U_{\text{trial}} = \frac{1}{2}\sum_{\mathbf{k}} G(\mathbf{k})|h(\mathbf{k})|^2 \tag{A.6}$$

where $G(\mathbf{k})$ is the unknown coupling coefficient in general mode-dependent form. Then, the total energy can be written as:

$$\mathcal{H} = \mathcal{H}_0 + \mathcal{H}_p = U_{\text{trial}} + (\mathcal{H}_0 + \mathcal{H}_p - U_{\text{trial}}) \tag{A.7}$$

Then the perturbation expansion of the free energy associated with the Hamiltonian in (A.7) is obtained by the Taylor series in (A.5):

$$F_\infty = F_0 - \frac{1}{\beta}\sum_{N=1}^{\infty} \frac{(-\beta)^N}{N!}\langle\left[\mathcal{H}_0 + \mathcal{H}_p - U_{\text{trial}}\right]^N\rangle^c_{U_{\text{trial}}} \tag{A.8}$$

where F_0 is the free energy corresponding to the trial Hamiltonian U_{trial}. Needless to say the full expansion in (A.8) as $N \to \infty$ *should be* independent of the choice of the trial Hamiltonian. In practice, however, the series is truncated up to a finite order M to

obtain an estimate of the free energy. Unlike the infinite series expansion in Eq. (A.8), the truncated series F_M *does* depend on the choice of the trial Hamiltonian $\mathcal{H}_{\text{trial}}$. Accordingly, in order to obtain an optimized estimate, we need to minimize the *sensitivity* of the truncated series to the trial Hamiltonian. To this end, we set (Kleinert, 2009):

$$\frac{\partial F_M}{\partial G(\mathbf{k})} := 0. \tag{A.9}$$

In a rather good approximation, the result for the truncated series of the variational free energy from this method will converge i.e. $F_M \approx F_{M+1}$ and achieves its minimal sensitivity to the trial function.

Data availability

No data was used for the research described in the article.

References

Abbena, E., Salamon, S., Gray, A., 2006. Modern Differential Geometry of Curves and Surfaces with Mathematica. CRC Press.

Ahmadpoor, F., Liu, L., Sharma, P., 2015. Thermal fluctuations and the minimum electrical field that can be detected by a biological membrane. J. Mech. Phys. Solids 78, 110–122.

Ahmadpoor, F., Sharma, P., 2016a. A perspective on the statistical mechanics of 2d materials. Extrem. Mech. Lett..

Ahmadpoor, F., Sharma, P., 2016b. Thermal fluctuations of vesicles and nonlinear curvature elasticity—implications for size-dependent renormalized bending rigidity and vesicle size distribution. Soft Matter 12 (9), 2523–2536.

Ahmadpoor, F., Wang, P., Huang, R., Sharma, P., 2017. Thermal fluctuations and effective bending stiffness of elastic thin sheets and graphene: A nonlinear analysis. J. Mech. Phys. Solids 107, 294–319.

Ahmadpoor, F., Zou, G., Gao, H., 2022. Entropic interactions of 2d materials with cellular membranes: Parallel versus perpendicular approaching modes. Mech. Mater. Accepted.

Akinwande, D., Brennan, C.J., Bunch, J.S., Egberts, P., Felts, J.R., Gao, H., Huang, R., Kim, J.-S., Li, T., Li, Y., et al., 2017. A review on mechanics and mechanical properties of 2d materials – graphene and beyond. Extrem. Mech. Lett..

Ares, P., Wang, Y.B., Woods, C.R., Dougherty, J., Fumagalli, L., Guinea, F., Davidovitch, B., Novoselov, K.S., 2021. Van der waals interaction affects wrinkle formation in two-dimensional materials. Proc. Natl. Acad. Sci. 118 (14), e2025870118.

Argudo, D., Purohit, P.K., 2014. Torsion of dna modeled as a heterogeneous fluctuating rod. J. Mech. Phys. Solids 62, 228–256.

Baczynski, K., Lipowsky, R., Kierfeld, J., 2007. Stretching of buckled filaments by thermal fluctuations. Phys. Rev. E—Stat. Nonlinear Soft Matter Phys. 76 (6), 061914.

Baizhikova, Z., Ballarini, R., Le, J.-L., 2024. Uncovering the dual role of dimensionless radius in buckling of spherical shells with random geometric imperfections. Proc. Natl. Acad. Sci. 121 (16), e2322415121.

Bianco, A., Kostarelos, K., Prato, M., 2005. Applications of carbon nanotubes in drug delivery. Curr. Opin. Chem. Biol. 9 (6), 674–679.

Biria, A., Maleki, M., Fried, E., 2013. Continuum theory for the edge of an open lipid bilayer. Adv. Appl. Mech. 21, 1–78.

Blees, M.K., Barnard, A.W., Rose, P.A., Roberts, S.P., McGill, K.L., Huang, P.Y., Ruyack, A.R., Kevek, J.W., Kobrin, B., Muller, D.A., et al., 2015. Graphene kirigami. Nature 524 (7564), 204–207.

Block, J., Witt, H., Candelli, A., Peterman, E.J.G., Wuite, G.J.L., Janshoff, A., Köster, S., 2017. Nonlinear loading-rate-dependent force response of individual vimentin intermediate filaments to applied strain. Phys. Rev. Lett. 118 (4), 048101.

Boal, D., Boal, D.H., 2012. Mechanics of the Cell. Cambridge University Press.

Bowick, M.J., Kosmrlj, A., Nelson, D.R., Sknepnek, R., 2017. Non-hookean statistical mechanics of clamped graphene ribbons. Phys. Rev. B 95 (10), 104109–NA.

Brangwynne, C.P., MacKintosh, F.C., Kumar, S., Geisse, N.A., Talbot, J., Mahadevan, L., Parker, K.K., Ingber, D.E., Weitz, D.A., 2006. Microtubules can bear enhanced compressive loads in living cells because of lateral reinforcement. J. Cell. Biol. 173 (5), 733–741.

Chaudhuri, O., Parekh, S.H., Fletcher, D.A., 2007. Reversible stress softening of actin networks. Nature 445, 295–298.

Chen, D., Kulkarni, Y., 2015. Entropic interaction between fluctuating twin boundaries. J. Mech. Phys. Solids 84, 59–71.

Chen, D., Kulkarni, Y., 2017. Thermal fluctuations as a computational microscope for studying crystalline interfaces: A mechanistic perspective. J. Appl. Mech. 84 (12).

Costa, K.D., Hucker, W.J., Yin, F.C.P., 2002. Buckling of actin stress fibers: a new wrinkle in the cytoskeletal tapestry. Cell Motil. Cytoskeleton 52 (4), 266–274.

Dai, Z., Lu, N., Liechti, K.M., Huang, R., 2020a. Mechanics at the interfaces of 2d materials: Challenges and opportunities. Curr. Opin. Solid State Mater. Sci. 24 (4), 100837.

Dai, Z., Sanchez, D.A., Brennan, C.J., Lu, N., 2020b. Radial buckle delamination around 2d material tents. J. Mech. Phys. Solids 137, 103843.

Dietz, H., Douglas, S.M., Shih, W.M., 2009. Folding dna into twisted and curved nanoscale shapes. Science 325 (5941), 725–730.

Euler, L., 1744. Methodus Inveniendi Lineas Curvas Maximi Minimive Proprietate Gaudentes Sive Solutio Problematis Isoperimetrici Latissimo Sensu Accepti. Marc-Michel Bousquet Co., Lausanne, Geneva.

Falvo, M.R., Clary, G.J., Taylor, R.M., Chi, V., Brooks, F.P., Washburn, S., Superfine, R., 1997. Bending and buckling of carbon nanotubes under large strain. Nature 389, 582–584.

Farokhirad, S., Kandy, S.K., Tsourkas, A., Ayyaswamy, P.S., Eckmann, D.M., Radhakrishnan, R., 2021. Biophysical considerations in the rational design and cellular targeting of flexible polymeric nanoparticles. Adv. Mater. Interfaces 8 (23), 2101290.

Feynman, R.P., Leighton, R.B., Sands, M., 1964. The Feynman Lectures on Physics. Vol. II, Addison-Wesley, Reading, Massachusetts.

Gao, W., Huang, R., 2014. Thermomechanics of monolayer graphene: Rippling, thermal expansion and elasticity. J. Mech. Phys. Solids 66, 42–58.

Gittes, F., Mickey, B., Nettleton, J., Howard, J., 1993. Flexural rigidity of microtubules and actin filaments measured from thermal fluctuations in shape. J. Cell. Biol. 120 (4), 923–934.

Gov, N., Zilman, A., Safran, S., 2003. Cytoskeleton confinement and tension of red blood cell membranes. Phys. Rev. Lett. 90 (22), 228101.

Grasinger, M., Sharma, P., 2024. Thermal fluctuations (eventually) unfold nanoscale origami. J. Mech. Phys. Solids 184, 105527.

Gurtin, M.E., Fried, E., Anand, L., 2010. The Mechanics and Thermodynamics of Continua. Cambridge University Press.

Hagerman, P.J., 1988. Flexibility of dna. Annu. Rev. Biophys. Biophys. Chem. 17, 265–286.

Hanakata, P.Z., Bhabesh, S.S., Bowick, M.J., Nelson, D.R., Yllanes, D., 2021. Thermal buckling and symmetry breaking in thin ribbons under compression. Extrem. Mech. Lett. 44, 101270.

Hassan, R., Farokhirad, S., Ahmadpoor, F., 2025. Entropic pressure between fluctuating membranes with surface tension. J. Appl. Mech. 1–9.

Hassan, R., Garzon, M.A., Gao, W., Ahmadpoor, F., 2024. Entropic pressure on fluctuating solid membranes. J. Mech. Phys. Solids 183, 105523.

Hutchinson, J.W., 2016. Buckling of spherical shells revisited. Proc. R. Soc. A: Math. Phys. Eng. Sci. 472 (2195), 20160577.

Kaisar, S., Hassan, R., Farokhirad, S., Ahmadpoor, F., 2025. Entropy-driven mechanics of crystalline and biological membranes. Appl. Mech. Rev. 1–23.
Kármán, T.V., 1907. Festigkeitsprobleme im maschinenbau. Mechanik 311–385.
Käs, J., Strey, H., Tang, J., Finger, D., Ezzell, R., Sackmann, E., Janmey, P., 1996. F-actin, a model polymer for semiflexible chains in dilute, semidilute, and liquid crystalline solutions. Biophys. J. 70 (2), 609–625.
Kittel, C., 2004. Elementary Statistical Physics. Courier Corporation.
Kleinert, H., 1989. Gauge Fields in Condensed Matter. Vol. 2, World Scientific, Singapore.
Kleinert, H., 2009. Path Integrals in Quantum Mechanics, Statistics, Polymer Physics, and Financial Markets. World Scientific.
Košmrlj, A., Nelson, D.R., 2016. Response of thermalized ribbons to pulling and bending. Phys. Rev. B 93 (12), 125431.
Kulkarni, Y., 2023. Fluctuations of active membranes with nonlinear curvature elasticity. J. Mech. Phys. Solids 173, 105240.
Kurachi, M., Hoshi, M., Tashiro, H., 1995. Buckling of a single microtubule by optical trapping forces: direct measurement of microtubule rigidity. Cell Motil. Cytoskeleton 30 (3), 221–228.
Landau, L.D., Lifshitz, E.M., 1986. Theory of Elasticity, third ed. Butterworth-Heinemann.
Lee, J.-H., Choi, S.-M., Doe, C., Faraone, A., Pincus, P.A., Kline, S.R., 2010. Thermal fluctuation and elasticity of lipid vesicles interacting with pore-forming peptides. Phys. Rev. Lett. 105 (3), 038101.
Lee, A., López Jiménez, F., Marthelot, J., Hutchinson, J.W., Reis, P.M., 2016. The geometric role of precisely engineered imperfections on the critical buckling load of spherical elastic shells. J. Appl. Mech. 83 (11).
Lipowsky, R., Leibler, S., 1986. Unbinding transitions of interacting membranes. Phys. Rev. Lett. 56 (23), 2541.
Lu, Q., Huang, R., 2009. Nonlinear mechanics of single-atomic-layer graphene sheets. Int. J. Appl. Mech. 1 (03), 443–467.
Morshedifard, A., Ruiz-García, M., Qomi, M.J.A., Košmrlj, A., 2021. Buckling of thermalized elastic sheets. J. Mech. Phys. Solids 149, 104296.
Nelson, David R., Peliti, L., 1987. Fluctuations in membranes with crystalline and hexatic order. J. Physique 48 (7), 1085–1092.
Nelson, D., Piran, T., Weinberg, S., 2004. Statistical Mechanics of Membranes and Surfaces. World Scientific.
Nicholl, R.J., Lavrik, N.V., Vlassiouk, I., Srijanto, B.R., Bolotin, K.I., 2017. Hidden area and mechanical nonlinearities in freestanding graphene. Phys. Rev. Lett. 118 (26), 266101.
Ramesh, S., Kulkarni, Y., 2024. Statistical mechanics of active vesicles and the size distribution paradox. J. Mech. Phys. Solids 191, 105749.
Shekhawat, A., Ritchie, R.O., 2016. Toughness and strength of nanocrystalline graphene. Nat. Commun. 7 (1), 1–8.
Singh, J., Purohit, P.K., 2020. Statistical mechanics of a double-stranded rod model for dna melting and elasticity. Soft Matter 16 (33), 7715–7726.
Su, T., Purohit, P.K., 2010. Thermomechanics of a heterogeneous fluctuating chain. J. Mech. Phys. Solids 58 (2), 164–186.
Su, T., Purohit, P.K., 2012. Semiflexible filament networks viewed as fluctuating beam-frames. Soft Matter 8 (17), 4664–4674.
Svenšek, D., Podgornik, R., 2008. Buckling of thermally fluctuating soft elastic rods. Phys. Rev. E 77 (3), 031808.
Timoshenko, S., 1983. History of Strength of Materials: With a Brief Account of the History of Theory of Elasticity and Theory of Structures. Courier Corporation.
Wang, Z., Tonderys, D., Leggett, S.E., Williams, E.K., Kiani, M.T., Steinberg, R.S., Qiu, Y., Wong, I.Y., Hurt, R.H., 2016. Wrinkled, wavelength-tunable graphene-based surface topographies for directing cell alignment and morphology. Carbon 97, 14–24.
Yap, H.S., Lakes, R.S., Carpick, R.W., 2007. Mechanical instabilities of individual multiwalled carbon nanotubes under cyclic axial compression. Nano Lett. 7 (5), 1149–1154.
Zelisko, M., Ahmadpoor, F., Gao, H., Sharma, P., 2017. Determining the gaussian modulus and edge properties of 2d materials: From graphene to lipid bilayers. Phys. Rev. Lett. 119 (6), 068002.
Zhang, T., Li, X., Gao, H., 2014. Designing graphene structures with controlled distributions of topological defects: A case study of toughness enhancement in graphene ruga. Extrem. Mech. Lett. 1, 3–8.